

## Investigations of the Mars upper atmosphere with Exomars Trace Gas Orbiter

Miguel A. López-Valverde<sup>1</sup> · Jean-Claude  
Gerard<sup>2</sup> · Francisco González-Galindo<sup>1</sup> ·  
Ann-Carine Vandaele<sup>3</sup> · Ian Thomas<sup>3</sup> ·  
Oleg Korablev<sup>4</sup> · Nikolai Ignatiev<sup>4</sup> ·  
Anna Fedorova<sup>4</sup> · Franck Montmessin<sup>5</sup> ·  
Anni Määttänen<sup>5</sup> · Sabrina Guilbon<sup>5</sup> ·  
Franck Lefevre<sup>6</sup> · Manish R. Patel<sup>7</sup> ·  
Sergio Jiménez-Monferrer<sup>1</sup> · Maya  
García-Comas<sup>1</sup> · Alejandro Cardesin<sup>8</sup> ·  
Colin F. Wilson<sup>9</sup> · R. T. Clancy<sup>10</sup> · Armin  
Kleinböhl<sup>11</sup> · Daniel J. McCleese<sup>11</sup> · David  
M. Kass<sup>11</sup> · Nick M. Schneider<sup>12</sup> · Michael  
S. Chaffin<sup>12</sup> · José Juan López-Moreno<sup>1</sup> ·  
Julio Rodríguez<sup>1</sup>

Received: date / Accepted: date

---

M. A. López-Valverde  
Instituto de Astrofísica de Andalucía/CSIC, Granada, Spain  
Tel.: +34-958-121311 , Fax: +34-958-814530 , E-mail: valverde@iaa.es

J.-C. Gerard  
Laboratoire de Physique Atmosphérique et Plantaire, Université de Liège, Belgium

F. González-Galindo, S. Jiménez-Monferrer and M. García-Comas and J. J. López-Moreno  
and J. Rodríguez  
IAA/CSIC, Granada, Spain

A.-C. Vandaele and I. Thomas  
IASB, Brussels, Belgium

O. Korablev and N. Ignatiev and A. Fedorova  
IKI, Moscow, Russia

F. Montmessin and A. Määttänen and S. Guilbon  
LATMOS/IPSL, UVSQ Université Paris-Saclay, UPMC Univ. Paris 06, CNRS, Guyancourt,  
France

F. Lefevre  
LATMOS/IPSL, UPMC Univ. Paris 06 Sorbonne Universités, UVSQ, CNRS, Paris, France

M. R. Patel  
Open University, Milton-Keynes, UK

A. Cardesin  
ESAC, Madrid, Spain

C. F. Wilson  
Physics Department, Oxford University, UK

R. Tood Clancy  
Space Science Institute, Boulder CO, USA

**Abstract** The Martian mesosphere and thermosphere, the region above about 60 km, is not the primary target of the Exomars 2016 mission but its Trace Gas Orbiter (TGO) can explore it and address many interesting issues, either in-situ during the aerobraking period or remotely during the regular mission. In the aerobraking phase TGO peeks into thermospheric densities and temperatures, in a broad range of latitudes and during a long continuous period. TGO carries two instruments designed for the detection of trace species, NOMAD and ACS, which will use the solar occultation technique. Their regular sounding at the terminator up to very high altitudes in many different molecular bands will represent the first time that an extensive and precise dataset of densities and hopefully temperatures are obtained at those altitudes and local times on Mars. But there are additional capabilities in TGO for studying the upper atmosphere of Mars, and we review them briefly. Our simulations suggest that airglow emissions from the UV to the IR might be observed outside the terminator. If eventually confirmed from orbit, they would supply new information about atmospheric dynamics and variability. However, their optimal exploitation requires a special spacecraft pointing, currently not considered in the regular operations but feasible in our opinion. We discuss the synergy between the TGO instruments, specially the wide spectral range achieved by combining them. We also encourage coordinated operations with other Mars-observing missions capable of supplying simultaneous measurements of its upper atmosphere.

**Keywords** Mars · Exomars · NOMAD · ACS · Upper Atmosphere · aerobraking · airglow · remote sounding

## 1 Introduction

Exomars 2016 was launched on March 14th, 2016, carrying two major modules: (i) the Trace Gas Orbiter, or TGO in short, a spacecraft in orbit around Mars with four remote sounding instruments on board, and (ii) the Schiaparelli surface platform. The release of the Schiaparelli module and the successful insertion of TGO into Mars orbit took place on October 19th, 2016 ([31]). A special period of high elliptic 4-sols (sol = Martian day) orbits around Mars immediately started, the so called Mars Capture Orbit phase (MCO hereinafter), which lasted for about two months. Around mid January 2017 maneuvers to change the orbit inclination and to lower the apocentre took place, shifting the orbital plane of TGO from the original nearly equatorial to a nearly polar orientation and reducing the period to about 1 day. In March 2017, a phase of aerobraking started, which will last for months, possibly until February 2018, when the regular operations should start. The final orbit will have a  $74^\circ$  inclination and a period of 2 h. The driving scientific goals of TGO and the individual instruments on-board can be found in several accompanying papers (Vandaele et al, 2017 [131]; Korablev et al., 2017 [72]).

The Martian mesosphere (altitudes between about 60 km and 120 km) and thermosphere (above about 120 km) are not the primary targets of the Exomars

---

A. Kleinböhl and D. J. McCleese and D. M. Kass  
JPL, Caltech, Pasadena, CA, USA

N. M. Schneider and M. S. Chaffin  
LASP, Boulder, CO, USA

2016 mission. However, this mission's instrumentation has capabilities to sound high in the Mars atmosphere, and the orbit configuration offers possibilities to address a number of open problems at high altitudes. Here we review these possibilities and their scientific interest, and try to motivate the Mars research community to pay attention to the upcoming data from the mission for exploiting them and to think about further upper atmosphere studies.

A short review of open problems in our understanding of the Mars upper atmosphere is discussed in Sect. 2 below. **This is a selection which does not aim to be exhaustive.** This work benefits from and builds upon a few recent and more extensive reviews written in preparation for the MAVEN mission (Bougher et al., 2014 [10]). We expect the Exomars 2016 TGO shall also contribute to some of the MAVEN goals and, further, to complement them in an altitude region not properly covered by MAVEN. In Sect. 3 we describe the nominal operations of TGO and a few simulations to illustrate the science that can be obtained from orbit with the key instruments. In Sect. 4 we discuss additional studies of the upper atmosphere that could be tackled with TGO, outside its standard operation modes. We will also propose observations to exploit the TGO instruments synergy, the aerobraking phase of the mission, as well as correlation campaigns with other instrumentation and projects, from the European Mars Express and the NASA missions Mars Reconnaissance Orbiter (MRO) and MAVEN, to the future James Webb Space Telescope (JWST in short). The major conclusions and recommendations are summarized in Sect. 5.

## 2 Brief review of Mars upper atmosphere's open questions

As reviewed by Leblanc et al, 2006 [74] (see references therein), five methods have been used so far to probe the Martian upper atmosphere, in-situ measurements, aerobraking and orbital decay, radio-occultation and remote sounding. In situ observations have been performed by descent probes like Viking and Pathfinder/ASIMET or the latest Schiaparelli/Exomars 2016. Accelerometer measurements of total density versus altitude have been performed during the aerobraking phase of several Mars orbiters, exploring atmospheric heights ranging from 110 to 180 km (Zurek et al., 2015 [147], Zurek et al., 2017 [146], Bougher et al., 2017 [9]). Radio occultation methods have provided the electron density profiles above 75 km, and remote sensing of airglow emissions of the upper atmosphere have been used since the early Mars missions (Bougher et al., 2017 [9] and references therein). Additionally, theoretical efforts have also focused in the development of numerical models of the upper atmosphere, tackling radiative (Wolff et al., 2017 [141], and references therein) and dynamical problems of the upper atmosphere (Bougher et al., 2014 [10] and references therein). Notably, the extension in altitude of the general circulation models now permits the global analysis from the surface to the exosphere, including links with the lower atmosphere (Bougher et al., 2006 [8], Spiga et al., 2012 [121], González-Galindo et al., 2015 [53], Bougher et al., 2015 [11]). The plethora of studies revealed, first of all, the need for more measurements and an example intended to fill in that need is the MAVEN mission (Jakosky et al., 2015 [63]). This mission is supplying a significant amount of new in-situ and remotely sensed measurements with its suite of instruments. This includes a mass spectrometer (NGIMS) for neutral and ion densities, a Langmuir probe (LPW)

for electron densities and temperatures, and an UV spectrograph (IUVS) yielding selected neutral and ion densities from dayglow emissions and stellar occultations. Here we paint a succinct panorama of half a dozen open and interesting issues in our understanding of the Mars upper atmosphere, which clearly demand further attention and which the TGO data may permit insightful analysis, both as a standalone experiment and as a new tool in combination with previous and future data.

I *EUV and non-EUV heating sources* The atmospheric heating by the solar flux in the extreme UV is the dominant heating source of the Martian thermosphere and the major driver of the daily variations. Still it is poorly described nowadays, with an essentially altitude-independent percentage of energy deposition based on theoretical studies in the 70s which require revision (Fox and Dalgarno, 1979 [40]). Such revision ideally should be based on new observations in a range of altitudes starting and above the mesopause (about 120-125 km on Mars). In the lower thermosphere in particular (120-160 km), where the strongest temperature gradient occurs, the atmospheric energy budget is complemented by diverse factors whose competing roles are not fully understood. These include radiation (emissions and solar absorptions in the IR and near-IR under non-local thermodynamic equilibrium), the global dynamics (inter-hemispheric transport of species and downwelling and diabatic heating in polar regions), and the small scale perturbations (waves and tides propagating up to thermospheric altitudes). TGO density and temperature determinations are expected in the whole mesosphere and lower thermosphere (MLT in short, 60-160 km), which should bring new data and impetus to this issue.

## II *Day/Night Changes*

Daily changes in the atmospheric basic structure (density and temperature) and composition are specially strong at the terminator (the day-night transition), and at high altitudes. They are part of the atmospheric natural variability and affect its structure at all altitudes above. Their precise understanding is important for reliable predictions for the aerobraking of orbiting satellites. Several open issues are closely related to local time variations; one example is the occurrence of CO<sub>2</sub> mesospheric clouds (González-Galindo et al., 2011 [54]). According to models, one of the two periods when the clouds are favored is during the first part of the Martian year around sunrise and sunset, when they are confined near the equator, where the thermal tides have largest amplitudes and produce temperature minima sufficiently close to the cold condensation values. As shown in Figure 1, the altitudes of temperature minima vary by 30 km between the two terminators **due to the thermal tides**. Day-night occurrences in clouds show a trend in agreement with the models, but the precise quantitative prediction at the terminator has not been confirmed by mesospheric cloud measurements given the incomplete local time coverage of previous satellite observations. Mesospheric clouds have also been observed in the daylight hemisphere by IUVS/MAVEN thanks to solar scattering in the UV (Deighan et al., 2017 [27]). The terminator will be described with unprecedented detail by TGO systematic observations from the ground up to the thermosphere. These TGO observations will nicely complement MAVEN measurements outside the terminator.

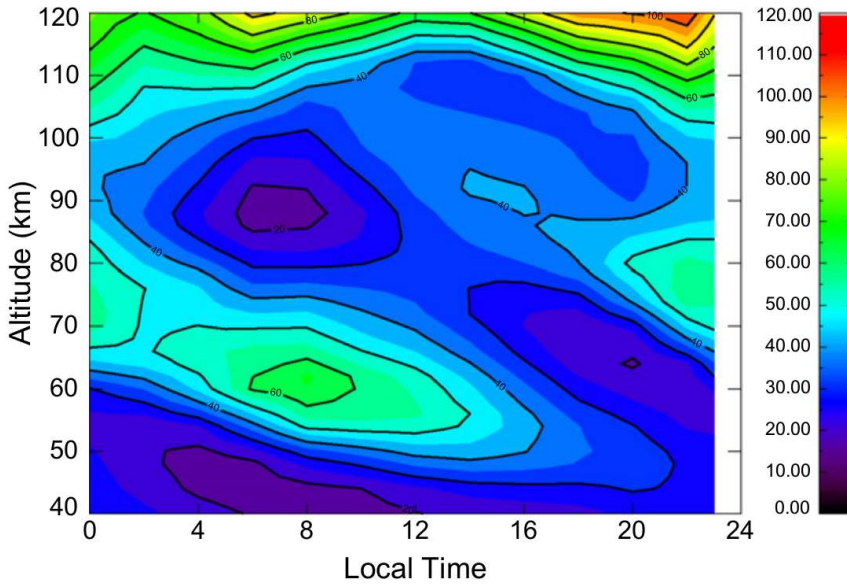


**Fig. 1** Difference between the atmospheric temperature and the condensation temperature of  $\text{CO}_2$ , as a function of altitude and local time, for ( $L_s=120$ – $150$ ,  $\text{Lon}=0$ ,  $\text{Lat}=0$ ), as simulated by the LMD-MarsGCM. After (González-Galindo et al., 2011 [54]).

### III Homopause/Mesopause variability

The location and temporal variation of these two layers are considered as prime indicators of our understanding of the upper atmosphere of the terrestrial planets, and certainly this is the case of Mars, now and during its long term evolution (Ehlmann et al., 2017 [29]). They depend on many dynamical and radiative processes, not only locally at their precise altitudes, or on the lower atmosphere below (Jakosky et al., 2017 [64]), but also on a global scale (González-Galindo et al., 2009 [52]). Further, they are key to understand processes like photochemical escape and the current atmosphere’s energy budget. The tracking of their variability requires systematic observations in the range of altitudes around 100–130 km on Mars (or an even wider range, according to Jakosky et al., 2017 [64]). This is possibly the coldest and most difficult region to sound, both from remote observations using emission spectroscopy and from in-situ satellite periapsis, normally at higher altitudes. Solar occultation observations present possibly the best tool to sound this atmospheric region. The deep-dips campaigns of MAVEN down to 120 km and the systematic mapping with TGO of the mesopause and homopause should complement and supply unique information to describe these critical layers.

### IV Wave coupling with lower atmosphere

The coupling of the lower and upper atmosphere occurs via propagation of waves, diffusion of species, the general circulation and local thermal expansion due to dust storms (Bougher et al., 2014 [10]). Gravity waves, tides and planetary waves at thermospheric altitudes were examined during the aer-

obraking of the MGS and MO spacecrafts (Forbes et al., 2002 [37]; Fritts et al., 2006 [41]) and more recently with MAVEN (Yigit et al., 2015 [145], Zurek et al., 2017 [146]). Density variations recently found as high as the exobase by MAVEN have been attributed to gravity waves (Yigit et al., 2015 [145]; Terada et al., 2017 [128]). Efforts have been also devoted recently to the parameterization of sub-grid scale gravity waves into GCMs (Yigit et al., 2008; Medvedev et al., 2015) and simulation of gravity wave propagation with mesoscale models (Spiga et al., 2012). Gravity waves may play an important role in the deposition of energy in the MLT region in Mars although their role on the global dynamics seems to be less important than it is on Earth (Bougher et al., 2006 [8]). Recent modeling of convectively driven gravity waves suggests that the propagation of short-period modes produced by vigorous convection can be so fast in the Martian atmosphere that such waves could reach even the upper thermosphere (Imamura et al., 2016 [61]). The propagation of gravity waves continues posing a challenge to models for two reasons. One is the intrinsic difficulty in the description of sources and propagation, both within 3-D global models and with 1-D constrained models. An example is the discussion over which, topography or convection, dominate the generation of these waves (Imamura et al., 2016 [61]). The other is the lack of measurements suited for their detection: in particular 2-D instantaneous mapping in the vertical and the horizontal, like that performed on Venus by VIRTIS/Venus Express; Gilli et al., 2009 [49], or like tomographic observations of the Earth's upper atmosphere (Song et al., 2017 [118]). The TGO long aerobraking phase and the systematic observations during solar occultation can be very valuable for this purpose. Furthermore, measurements during non-nominal operation modes, as those proposed in section 4.2, could also be very informative to describe further the small-period gravity waves.

#### V *Photochemistry and escape of water vapor*

As discussed by Bougher et al. 2014 [10]) regular observations of the neutral species are needed to understand escape processes, in addition to their variability with local times, latitudes and seasons, and the solar cycle. This is the case of the light species which form the Martian corona, or exosphere, and their escape rates. One of the all important species is H and the D/H ratio, linked to the escape of water vapor, which in the classical photochemical frame, takes place first by diffusion of H<sub>2</sub> upwards to the homopause layer, and then throughout the thermosphere, preferentially in the atomic form (Clarke et al., 2014 [22]). Recent measurements of H and D abundances by IUUV/MAVEN in the far-UV (Chaffin et al., 2014 [14]; Clarke et al., 2017 [23]) show large variations of both H and D Lyman alpha emissions, with excursions up to very high D/H ratios at thermospheric altitudes over the course of a Martian year, well above the value  $\sim 5$  found at low altitudes. The variations contain a clear seasonal component which is not entirely explained in terms of EUV solar radiation (Chaufray et al., 2015 [15]). Tentative explanations propose elevated H<sub>2</sub>O abundance at mesospheric altitudes, perhaps linked to a convectively active lower atmosphere (Fedorova et al., 2015 [33]). The critical mesospheric and lower thermospheric altitudes will be systematically sounded by TGO, and further, it is expected to measure D/H ratios and H<sub>2</sub>O abundance profiles with unprecedented precision. These

results, together with recent determinations by instruments like IUVS and NGIMS on MAVEN, should be crucial for our understanding of the escape of water, including the challenging lower-to-upper atmosphere diffusion and its implications for the long term escape and evolution of species like water on Mars.

#### VI *Airglow and non-thermal emissions*

Airglow emissions in the UV and visible, together with IR emissions under non-local thermodynamic equilibrium situations, are distinct features of the upper atmospheres of the terrestrial planets. They strongly depend on key geophysical parameters, like temperature and species abundances and atmospheric chemistry (and therefore escape), but also on solar inputs (radiant fluxes and particle precipitation), photochemical reactions and ionization, and molecular energy transfer processes. The upper atmospheres are natural laboratories where much can be learned about all these parameters and processes, and viceversa, their emission rates are key ingredients in the radiative balance at high altitudes (Barth et al., 1992 [3], Strobel, 2002 [127], Lopez-Puertas and Taylor, 2001 [80]). Understanding these emissions is the goal of a large number of aeronomic studies carried out in particular on Mars since the early days, and many of them have been mentioned above. Many efforts have been devoted to their theoretical modeling, while on the experimental side, breakthrough investigations have been performed from ground-based observations and from most space missions around Mars (see the reviews by Bougher et al., 2014 [10], and also those by Wolff et al., 2017 [141], and Bougher et al., 2017 [9] in the recent compendium “The Atmosphere and Climate of Mars” [1], and references therein). TGO represents a new opportunity to continue learning about the origin and the variability of these emissions. We will address some of the most interesting airglow emissions and the related science possibilities in the following sections.

#### VII *Current challenges for Global Climate Models*

Physical models and numerical simulations need to be confronted and validated with data, and in a systematic manner whenever possible. This is particularly needed in the Martian upper atmosphere, where current predictions by global models present outstanding discrepancies. **Although previous sections already discuss diverse challenges to GCMs, we want to recall here** discrepancies on the mean state and on the variability at high altitudes, this lasts one specially not well represented by the GCMs. One recent example is the density variations observed in-situ by the MAVEN accelerometers during the deep-dip campaigns, specifically around the terminators (Zurek et al., 2017 [146]). Another result is the NO nightglow observed by IUVS/MAVEN in the Northern Hemisphere winter and low-mid latitudes, much stronger than model predictions for those conditions (Stiepen et al., 2017 [126]). And a third discrepancy is the global temperatures in the mesopause region (110-130 km), much colder than what Martian ground-to-thermosphere GCMs predict (Medvedev et al., 2015 [96]; González-Galindo et al., 2017 [55]). Still we rely on GCM predictions to design space instrumentation and aerobraking maneuvers, and to complete the disperse map of measurements. Datasets like the Mars Climate Database (Millour et al., 2015 [98]) and Mars-GRAM (Justh et al., 2011 [65]),

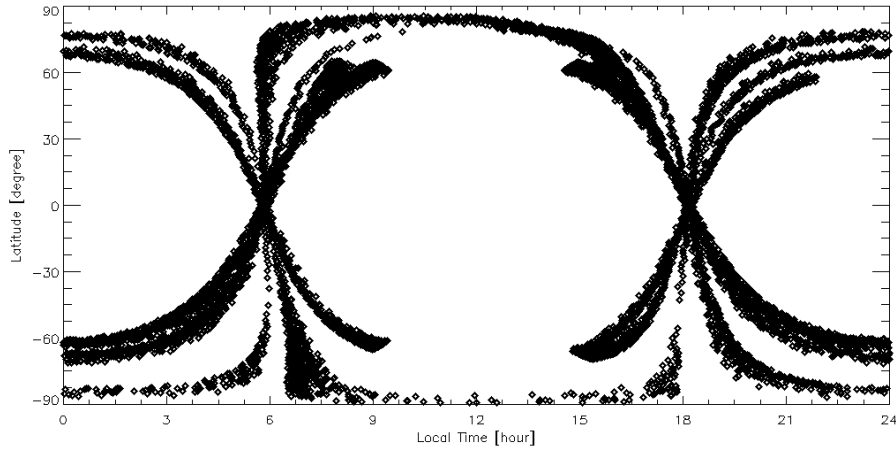


**Fig. 2** Location in a Latitude-Local Time map of the solar occultations expected during the whole 2018.

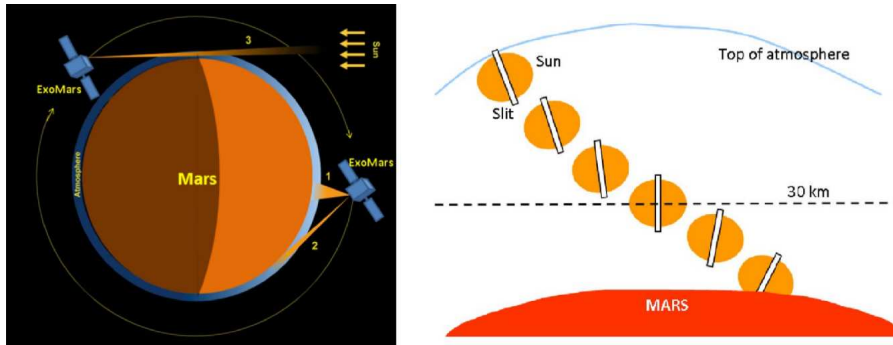


**Fig. 3** Schematic diagram of the NOMAD and ACS observation modes, extracted from Neefs et al., 2015 [105], with permission. Only the NOMAD-SO slit is shown, and its projected length is about the size of the Sun's disc. The ACS-MIR slit is smaller, parallel to the NOMAD-SO and located near its center, and the ACS-NIR is perpendicular and about 4 times larger.

based on GCMs simulations, are under continuous validation from new missions, and TGO will supply a new and unique dataset with a focus on the day-night transition and a wide range of local times at high latitudes which are novel and valuable for model validation purposes. The latitude and local time coverage expected for 2018 are shown in Figure 2.

### 3 TGO Nominal operations

The Nadir and Occultation for Mars Discovery (NOMAD) and the Atmospheric Chemistry Suite (ACS) are the two key instruments on board TGO for trace gas

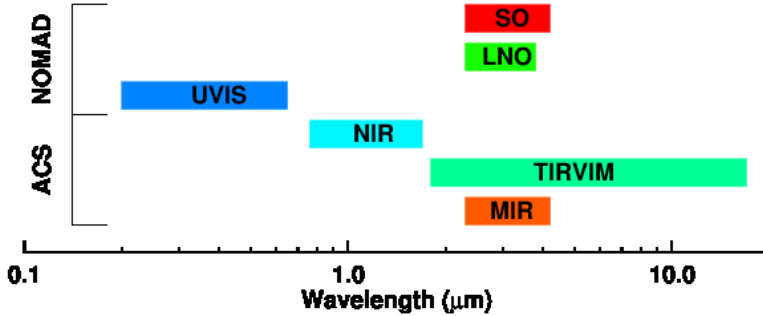


**Fig. 4** Spectral coverage obtained combining the NOMAD and ACS channels. The six channels are described in Table 1

detection and mapping. Both will be observing the Mars atmosphere using solar occultation and nadir mapping, as illustrated in Figure 3. The TGO nominal orbit, nearly circular at 380-420 km altitude, will have a typical sub-track velocity of 3.4 km/s and an orbital period of about 2 hours.

NOMAD has three separate optical layouts and detectors, which supply three signals: the “solar occultation” (or SO in short), the “limb-nadir-occultation” channel (LNO in short) and a UV channel (UVIS), whose characteristics are described by Vandaele et al., 2015 [133], Thomas et al., 2016 [129], Robert et al., 2016 [112], Patel et al., 2017 [106] and by Vandaele et al., 2017 [131] (this issue). A summary is listed in Table 1. The SO is only used for solar occultation; the LNO has a movable mirror which permits to point towards nadir or towards the limb (co-aligned with the SO line of sight), and could perform solar occultations; and the UV channel can also perform nadir and limb pointing, with a broad and a narrow field of view, respectively. Both SO and LNO use an acousto-optical filter (AOTF) in combination to the echelle grating in order to select diffraction orders (Neefs et al., 2015 [105]), of typical widths about  $20\text{-}35\text{ cm}^{-1}$ , i.e., about 100 different diffraction orders are defined for the two channels. Their measurements are performed in cycles which typically are 1 s for SO during solar occultation and 15 s for LNO during nadir mapping. Up to six different AOTF settings or diffraction orders are permitted during each solar occultation cycle and up to three during nadir observations (Vandaele et al., 2017 [131]). The detectors in both IR channels contain 320 columns (spectral direction) by 256 rows of pixels (spatial direction), and NOMAD is flexible regarding pixel binning, in order to reach a compromise

**Table 1** NOMAD and ACS channels' characteristics

Instrument & Channel	Range ( $\mu\text{m}$ )	Resolution ( $\text{cm}^{-1}$ )	LIMB FOV <sup>Ⓝ</sup>	NADIR Footprint <sup>Ⓝ</sup>	
NOMAD	SO	2.2 - 4.2	0.15 - 0.22	1 x 14	
	LNO	2.3 - 3.8	0.3 - 0.5	2 x 67	
	UVIS	0.2 - 0.65	$\sim 1.5$ nm	1 x 1	
ACS	NIR	0.76 - 1.6	0.4	5 x 50	
	MIR	2.3 - 4.3	0.085	0.5 x 7.5	
	TIRVIM	2 - 17	0.25-1.3	70 x 70	
		SNR <sup>†</sup>	NESR <sup>♡</sup>		Integration Time <sup>⊗</sup>
NOMAD	SO	2000	$8 \times 10^{-10}$		1
	LNO	100 - 3000	$\sim 2 \times 10^{-8} - 6 \times 10^{-10}$		1 - 15
	UVIS	500 - 500	$10 - 10^{-6}$ (★)		1 - 15
ACS	NIR	100 - 4000	$5 \times 10^{-7} - 4.5 \times 10^{-10}$		0.05 - 5
	MIR	3500	$5 \times 10^{-10}$		0.5 - 2
	TIRVIM	1500 - 50	$\sim 2 \times 10^{-8} - 10^{-9}$ (♣)		1.8 - 6.6

<sup>Ⓝ</sup> Units: km. Adapted from Table 1 in Roberts et al., 2016 [112] and Korablev et al., 2015 [73]

<sup>⊗</sup> These are typical integration times in seconds for solar occultation (SO, UVIS, MIR, NIR, TIRVIM) and for nadir mapping (LNO, UVIS, NIR, TIRVIM) from Neefs et al., 2015 [105], Patel et al., 2017 [106] and Korablev et al., 2017 [72].

<sup>†</sup> These are expected values for typical integration times, at the center of the spectral order and for nominal working temperatures. SNR values for NOMAD LNO and SO could improve with the number of accumulations and level of pixel binning (Neefs et al., 2015 [105]). For NIR in nadir mode, the SNR can increase by averaging of lines inside the slit. The MIR SNR can also increase with the number of accumulation of frames.

<sup>♡</sup> Noise Spectral Equivalent Radiance units:  $W/cm^2/cm^{-1}/sr$ . Estimations for NOMAD based on the radiometric model of the instrument (Thomas et al., 2016 [129]) and the nominal integration times (Robert et al., 2016 [112]); see also Vandaele et al., 2017 [131]. Values for ACS are based on Korablev et al., 2017 [72]. See text for details.

(★) The extremely diverse values of 10 and  $10^{-6}$  correspond to nadir mapping and solar occultation, respectively.

(♣) The NESR value of  $10^{-9}$  for TIRVIM for solar occultation is an estimation using approximate values of solar inputs used in the NOMAD LNO characterization (from Vandaele et al., 2017 [131]) and therefore only valid in the TIRVIM lowest wavelength range, 2-4  $\mu\text{m}$ .

between SNR and spectral resolution. UVIS records the whole 200-650 nm spectrum at once, can perform observations with integration times between 50 ms to 15 s, and like SO and LNO, admits pixel (spectral) binning to increase SNR (Vandaele et al., 2015 [133]; Patel et al., 2017 [106]).

ACS is a set of three spectrometers whose combination cover from the near IR (0.7  $\mu\text{m}$ ) to the thermal IR range (17  $\mu\text{m}$ ) with spectral resolution and other characteristics as listed in Table 1 (Korablev et al., 2015 [73] and Korablev et al., 2017 [72] in this issue). Some caution is needed regarding the values of the Noise Equivalent Spectral Radiance (NESR) in Table 1. The ACS and NOMAD channels have performed in-flight calibration during the Mid-Cruise check-up and the Mars Capture Orbit campaigns, however, the NESR values have not been yet obtained for all the observations modes and all the NOMAD and ACS channels. For some of the modes we have estimated the NESR for one instrument using inputs for solar fluxes and nadir radiances from simulations for the other. Giving one single NESR value is an oversimplification because the nadir signal changes significantly with the very variable dust opacity and surface albedo (Robert et al, 2016 [112]). The

same for the solar occultation, which will not be completely characterized until regular occultations are performed from the final orbit with both instruments.

The ACS MIR channel is an echelle spectrometer devoted to solar occultation only, including a secondary dispersion element to fill-in a 2-D detector array. Its full spectral range is sampled by the different echelle orders (in the x-axis of the detector) and by rotating the secondary grating (introducing the separation into the y-axis). During a solar occultation only 1 or 2 positions of the secondary grating are used, i.e., two spectral sub-domains, which allows for up to  $0.3 \mu\text{m}$  per measurement. The ACS NIR is a similar concept to the NOMAD SO and LNO channels, i.e., it is an echelle spectrometer and an acousto-optical tunnable filter to sample the different orders. The orders are narrow but up to 10 different orders can be used sequentially during a single observation. The ACS TIRVIM is “the” infrared instrument of TGO, with a very wide spectral range,  $2\text{--}17 \mu\text{m}$ . It is a double-pendulum Fourier transform spectrometer with two ranges of the swing movement. The first, a full swing range, gives a better spectral resolution and is used for solar occultation. The second one, a reduced swing movement, has a lower spectral resolution and is intended for nadir mapping. For proper radiometric calibration during nadir sounding, TIRVIM includes an internal blackbody. As with the LNO and UVIS channel, the NIR and TIRVIM channels have two optical ports and are therefore versatile in pointing possibilities, including nadir and solar occultations, and even limb observations off the terminator (measurements in emission), if these were performed (see Section 4.2 below). In practice, however, their actual sensitivities may preclude certain observations, and this is the case of the expected TIRVIM signals in nadir from Mars orbit in the lowest wavelength range ( $1.7\text{--}5 \mu\text{m}$ ). This TIRVIM spectral region may be suitable for solar occultation, while the nadir mapping shall be carried out in the TIRVIM longest wavelength range (Korablev et al., 2017 [72]). Notice that in the overlapped spectral region between MIR and TIRVIM, i.e.,  $2.3\text{--}4 \mu\text{m}$ , the MIR spectral resolution and sensitivity are better than the TIRVIM counterparts. However, at longer wavelengths, beyond the MIR range, solar occultation with TIRVIM offers interesting possibilities for trace gas detection of species like  $\text{H}_2\text{O}_2$  (at  $7.7 \mu\text{m}$ ) in the lower atmosphere, and  $\text{O}_3$  ( $9.6 \mu\text{m}$ ),  $\text{CO}$  ( $4.7 \mu\text{m}$ ) and  $\text{NO}$  ( $5.3 \mu\text{m}$ ) up to mesospheric altitudes.

There is a clear synergy between both instruments, with redundant spectral regions (around the  $3.3 \mu\text{m}$  band of  $\text{CH}_4$  for example) and with complementary spectral coverage, namely the UVIS signal of NOMAD and the thermal infrared channel (TIRVIM in short) of ACS. Together they cover, almost continuously, a very broad spectral range, from the UV to the far IR, as illustrated in Figure 4. However, as explained above, the different channels, and therefore, the different spectral ranges will combine differently in the two standard science or pointing modes: SO, UVIS and MIR can observe during solar occultation (during sunsets and sunrises, at the terminators), and LNO, UVIS, NIR and TIRVIM can operate during nadir mapping (daytime and nighttime). SO and UVIS can be operated simultaneously with NIR and TIRVIM, to achieve a wide spectral coverage; unfortunately ACS-MIR cannot perform solar occultations at the same time as the NOMAD channels due to a difference of boresight alignment. Nearly simultaneous solar occultation by both instruments will supply mutual validation of the SO and MIR channels and redundant measurements of the key trace species in the near-IR. Notice that, as shown in Figure 3, the NIR slit is parallel to the planet’s limb while the SO is perpendicular. The vertical resolution and sampling in the

SO signal will depend on the binning of detector rows (spatial dimension), which can be modified via telecommanding; for the minimal number of 4 rows binned the best vertical sampling and resolution corresponds to about 0.5 km (Vandaele et al., 2017 [131]), much better than typical scale heights of all species of interest.

The major goals of NOMAD and ACS coincide with the primary objectives of Exomars 2016, which are the detection of trace species and the mapping of their spatial and temporal distribution. They have been extensively described by Vandaele et al., 2015 [132] and Korablev et al., 2015 [73]; see also Korablev et al., 2017 [72] and Vandaele et al., 2017 [131] in this issue. Regarding the upper atmosphere, and as discussed by Vandaele et al., 2015 [132], the primary targets are the lower-to-upper atmosphere dynamical and chemical coupling, including escape processes, as well as the improvement of upper atmosphere’s climatologies. To achieve these goals, the key task is the derivation of vertical profiles of densities of several species, which by combining NOMAD and ACS they include CO<sub>2</sub>, CO, O<sub>3</sub> and H<sub>2</sub>O in the IR, O<sub>2</sub> in the visible, and aerosols in the UV. NOMAD and ACS have the combined ability to examine the UV–to–IR varying scattering properties in order to separate dust from ice aerosols (Vandaele et al., 2017 [131]). Atmospheric temperatures at high altitudes should be derived directly from the rotational structure of some bands (notably CO<sub>2</sub> and CO), or indirectly, from the scale heights of the density profiles assuming hydrostatic equilibrium. These two methods are completely independent and both have been applied previously to solar occultations measurements in the Venus atmosphere by SPICAM/SOIR on Venus Express; their agreement within noise limits confirmed the values obtained and served as a mutual validation (Piccialli et al., 2015 [109]; Mahieux et al., 2015 [91]). Further, the combination of the thermal profiles with those obtained in the lower atmosphere during the nadir mapping with TIRVIM at 15  $\mu\text{m}$  will characterize the thermal regime from the ground to the thermosphere, although not with a perfect 1-D description but rather as a statistical combination of spatially and temporally comparable data. The impact of all these results on the extension of existing databases of composition, temperature and aerosol loading at high altitudes will be very significant and represent the first benefit from this mission for our understanding of the Mars upper atmosphere.

### 3.1 Solar occultation

Solar occultation is the most precise remote observation strategy that can be used to sound as high as possible in an atmosphere. The combination of a strong source and a limb grazing path permits the maximum sensitivity to weak absorption bands and trace species, more difficult to observe otherwise. Ideal additional characteristics of an upper atmosphere sounder are high detector sensitivity, good spectral resolution, and high versatility in pointing.

Regular TGO observations at the terminator, from both NOMAD and ACS, are expected to supply observations during 1 sunset and 1 sunrise each orbit, i.e., each 2 hours approximately. During a solar occultation the size of the Sun is 21’, or 11 km if projected onto the limb; the time for crossing a 100 km atmosphere is about 60 s, with a maximum descent velocity of 2 km/s. The 12 orbits per Martian day (sol) in the regular science phase amount to typically 56 solar occultations per sol. The distribution with latitude and season of the resulting mapping is shown

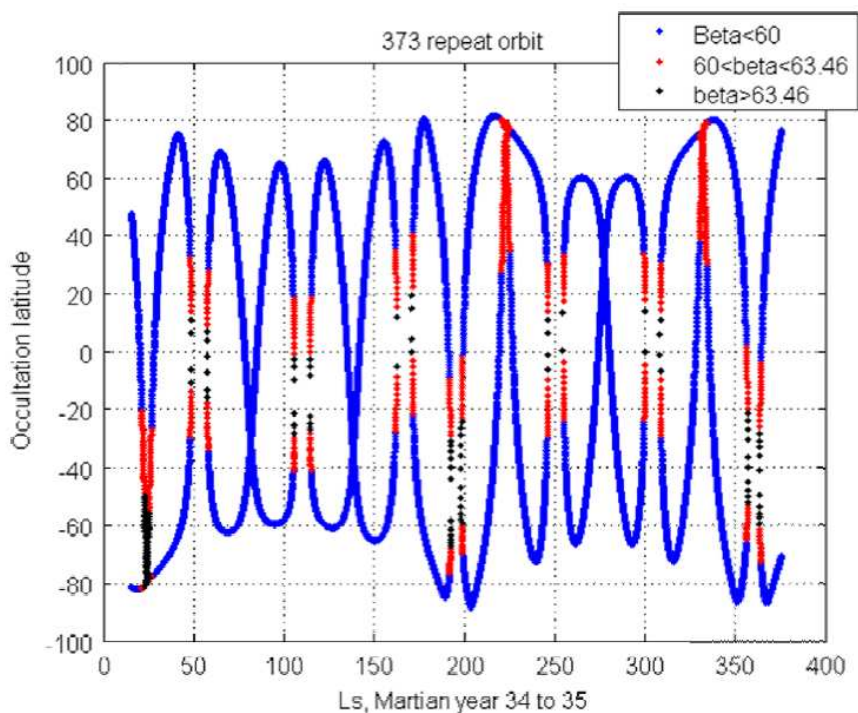


**Fig. 5** Location in a Latitude-Solar Longitude map of the solar occultations during one Martian year. The beta angle is expressed in degree and represents the inclination of the Sun vector over the plane of the TGO orbit.

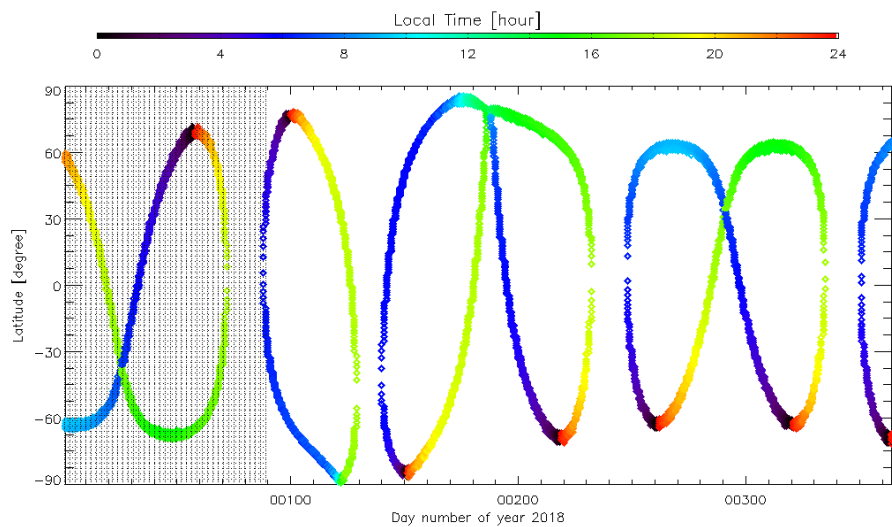


**Fig. 6** Similar to Figure 5 but applied to the whole 2018 and adding in colors the local time variability (see Figure 2). The shaded area corresponds to the first three months of the year, probably not available for routine operations. See text.

in Figure 5 and described by Vandaele et al., 2015 [132]. The Local Time coverage is close to 6 am and 6 pm at the equator and wider at higher latitudes as shown in Figure 2 above; notice however that latitudes between  $\pm 40^\circ$  are hardly explored, unless the periods of high beta angle are exploited. This possibility would add potential for studying phenomena confined to equatorial latitudes, like CO<sub>2</sub> mesospheric clouds (González-Galindo et al., 2011 [54]). The combination of local time and latitude locations is shown in Figure 6 for the year 2018, as an example of the complex variability which will pose a challenge for their interpretation. Notice that many different longitudes are combined in this map at every latitude, but this map can be used to propose observations mostly dependent on local time, like the study of migrating tides and their effects at high altitudes. As mentioned above, we also expect other interesting changes during the Martian day, including different day/night abundance of several chemical species (odd oxygen and hydrogen families) and of excited species (CO<sub>2</sub>, O(1D), and other photolysis products). Further, the global dynamics at high latitudes impose a strong variability in global densities (CO<sub>2</sub>) and in the transport of species, specially in the upper atmosphere (González-Galindo et al., 2015 [53]). We therefore expect to test Mars global models and to learn a lot about these atmospheric variabilities from the upcoming TGO solar occultations.

With such a dataset, we particularly expect to fill in the important altitude range from 80 km, nominal top altitude of the MCS/MRO experiment, up to the upper thermosphere. The precise uppermost altitude expected from each TGO instrument can be evaluated with a detailed line-by-line calculation of atmospheric transmittances together with a realistic estimation of the instrumental noise. Next we analyze this for the different NOMAD and ACS channels.

### 3.1.1 NOMAD and ACS IR channels

Figure 7 shows such a calculation in the IR, specifically in the 2.5-2.9  $\mu\text{m}$  region for an arbitrary reference atmosphere extracted from the Mars Climate Database. The line-by-line transmittances were convolved with an approximate instrumental response at 0.15  $\text{cm}^{-1}$  resolution, to mimic the NOMAD SO signal, as was done by Vandaele et al., 2015 [132] in similar transmittance calculations but at tangent heights below 50 km. Using a conservative estimation of the SNR of 2500 for the SO channel (Robert et al., 2016 [112]), consistent with the NESR value shown in Table 1, all the spectral features visible in figure 7, even at 170 km altitude (**about 0.05 nbar in this reference atmosphere**), should be detected in the SO signal. Since the ACS MIR has a spectral resolution about 3 times better than the SO channel but a lower sensitivity by about the same factor, the same conclusion applies to the solar occultation with ACS/MIR.

Figure 8 shows that these sensitivity levels are excellent to detect “hot bands” of CO<sub>2</sub>; the First Hot band of the major isotope (626) in particular should be clearly seen at altitudes well above 130 km (**at least up to about 150 km, or equivalently to CO<sub>2</sub> number densities around  $10^{10} \text{ cm}^{-3}$ , for this model atmosphere and the assumed SNR value**). This is very interesting for non-local thermodynamic equilibrium studies (non-LTE). Emission spectroscopy is very useful to study the excited states of molecules like CO<sub>2</sub> which may present strong non-LTE populations, but is subject to diverse uncertainties. These include collisional

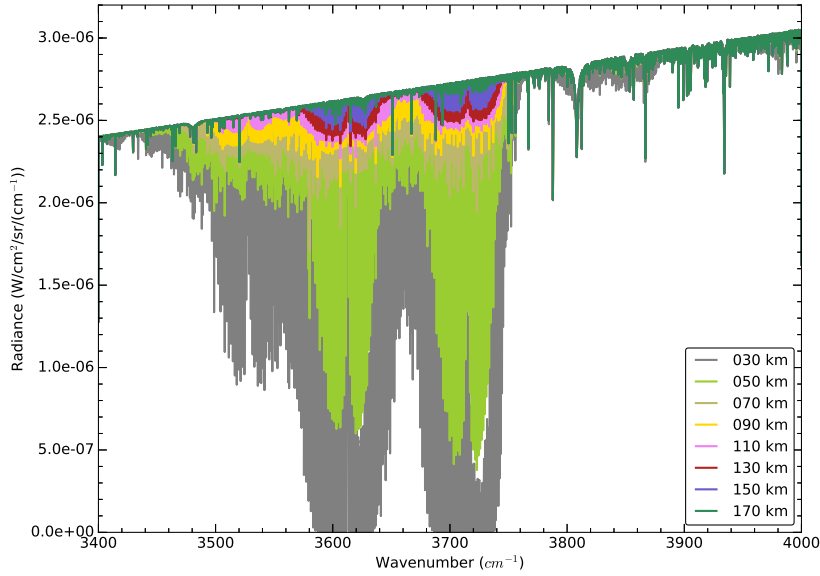


**Fig. 7** Simulation of the solar radiance expected in the NOMAD LNO and ACS MIR channels at different tangent altitudes, as indicated, and for a typical Martian reference atmosphere.

rate coefficients poorly constrained in laboratory and which therefore require assumptions and approximations (López-Valverde and López-Puertas, 1994a [83]; López-Puertas and Taylor, 2001 [80]). Absorption spectroscopy, on the contrary, sounds the lower state of the transitions and is more free from those modeling uncertainties. The lower state is the ground state in the fundamental bands, but for hot bands it is an excited state. Figure 8 shows LTE-NLTE differences of simulated transmittances to illustrate how the NOMAD SO measurements should permit the study of the population of the lower state of the First Hot band, the (010) state. This is expected to separate from LTE in the upper mesosphere and the whole thermosphere during daytime (López-Valverde and López-Puertas, 1994b [82]), and these data combined with the total density of  $\text{CO}_2$  would supply a direct measurement of the (010) state population, a direct test for the non-LTE models. *Let us recall that these models supply one of the two key ingredients of the Martian radiative balance at thermospheric altitudes, i.e., the thermal cooling at  $15\text{-}\mu\text{m}$ , the other one being the EUV solar heating mentioned in section 2.*

Figure 9 shows this detection capability more clearly in a narrow region around  $2.83\ \mu\text{m}$ , where the  $\text{CO}_2\text{-}636$  isotope has its strongest absorption lines. In this figure the irradiance shown is not the actual flux level observed but the difference from the flux at the top of the atmosphere (TOA). Individual lines from diverse  $\text{CO}_2$  bands and isotopes show a funny shape due to the log scale used. If the expected noise level is confirmed, the isotopic 636 lines should be detected below about 150

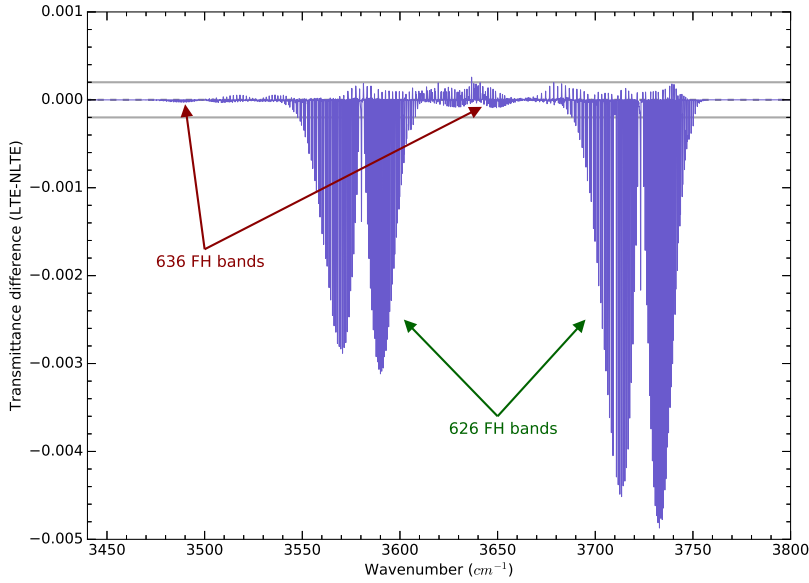


**Fig. 8** Simulation of the atmospheric transmittance differences LTE-NLTE by the “First Hot” (FH) band of the two main CO<sub>2</sub> isotopes, 626 and 636, as indicated, at a tangent altitude of 130 km for the reference atmosphere used in this work. A line for a SNR=5000 is indicated for reference. See text for details.

km. We can also see lines of the First Hot (FH) band of the main CO<sub>2</sub> isotope (626) in the upper mesosphere and below.

Other CO<sub>2</sub> and CO ro-vibrational bands in the near-IR range [1.0-2.0]  $\mu\text{m}$ , which can be covered by the ACS-NIR instrument will also be useful for sounding although up to lower altitudes. The strongest CO<sub>2</sub> band in this range, at 1.43  $\mu\text{m}$ , about 1000 times weaker than the 2.7  $\mu\text{m}$  bands, was used to derive CO<sub>2</sub> up to 90 km by Fedorova et al., 2009 [35] during solar occultations with SPICAM. Similar or higher altitudes should be achieved with NIR, given its better SNR and spectral resolution. The interest of using this band is the simultaneous derivation of H<sub>2</sub>O from the nearby band at 1.38  $\mu\text{m}$ , as exploited by SPICAM (Fedorova et al., 2009 [35]). The CO overtone band at 2.3  $\mu\text{m}$  could be detected in single CO measurements by NOMAD and ACS at least below about 75 km under dust free conditions, with one single solar occultation, and perhaps up to the mesopause (Korablev et al., 2017 [72]). Also its fundamental at 4.7  $\mu\text{m}$  band could be detected up to the lower thermosphere with TIRVIM during solar occultation. These are estimates extrapolating the sensitivity study of the NOMAD IR channels at 20 km tangent height by Robert et al., 2016 [112].

Further in the IR region, other molecules like nitric oxide have emission bands, at 5.3 and 7.6  $\mu\text{m}$ , which should also be detected in solar occultation with TIRVIM. For details of the TIRVIM detection limits for different species we refer the reader to the companion paper by Korablev et al., 2017 [72] in this issue.

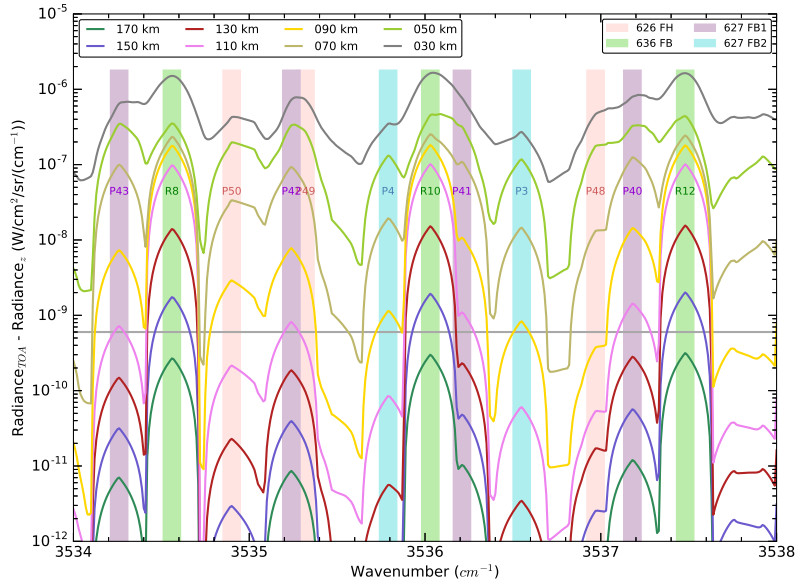


**Fig. 9** Simulation of the difference between the solar spectral irradiance at each tangent altitude and that at TOA. Different colors are used to visualize the different tangent altitudes. The gray line is the nominal noise of the NOMAD SO channel. Positions of individual lines and bands are indicated with arrows. “FH” and “FB” stand for First Hot and Fundamental Bands. See text for details.

*Atmospheric thermal structure* Atmospheric temperature profiles can also be obtained from the scale height of the species densities. Examples of similar studies using limb observations are the analysis of SPICAM stellar occultations in the UV by Forget et al. (2007) [38] and the retrieval of the Venus thermal structure from SPICAV stellar occultations (Piccialli et al., 2015 [109]) and from SOIR solar occultations (Mahieux et al., 2010 [92], Mahieux et al., 2015a [90]). The spectral resolution might not be enough to derive atmospheric temperatures directly from the rotational distribution of all the bands, although this was possible with SOIR on board Venus Express (VEx) in a few cases (Mahieux et al., 2015 [91]). Given the similarity and heritage between NOMAD and SOIR, and despite the different FOV and integration times, similar vertical resolution in the temperature retrieval is expected, which means close to the sampling, i.e., about 1 km for integration times of 1 s (Vandaele et al., 2017 [131]).

### 3.1.2 NOMAD UVIS channel

In the UV part of the spectrum, 200-650 nm, the solar occultation with UVIS is expected to map ozone and aerosols, as has been done with SPICAM similar observations in the past (Määttä et al., 2013 [86]). Both ozone and aerosols have indirect implications for the upper atmosphere, via photochemistry and radiation.

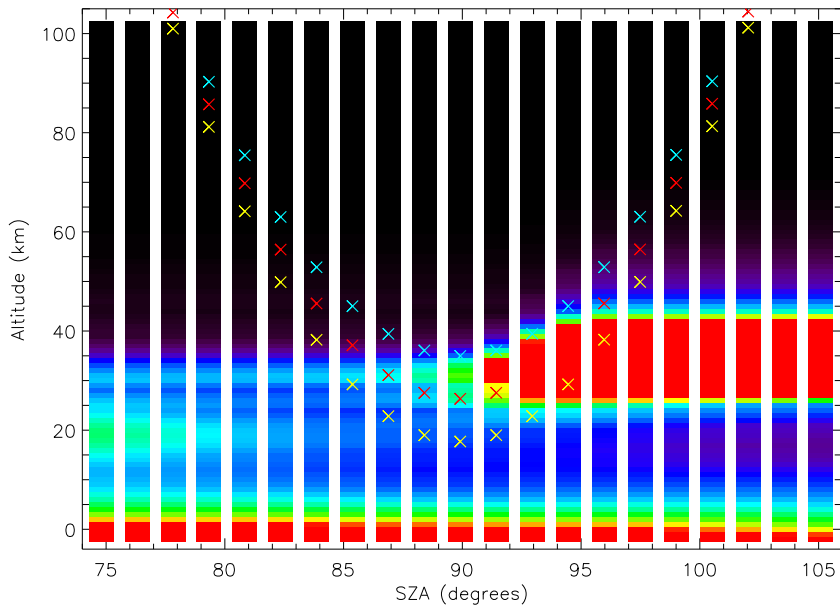


**Fig. 10** The vertical distribution of ozone as a function of the solar zenith angle (SZA) simulated by the LMD Mars global climate model for a chosen solar occultation by SPICAM. Three lines-of-sight with tangent altitudes of 20, 30 and 40 km of the SPICAM occultation are overplotted with symbols (yellow, red and blue crosses). The color scale goes from 0 to  $8 \times 10^{14} m^{-3}$ . The colors of the crosses in the lines-of-sight do not follow the abundance's color scale; they are simply fixed for clarity.

*Ozone* Ozone has been profiled in the Martian atmosphere up to the altitude of 50 km by SPICAM on board Mars Express (Lebonnois et al. 2006 [75], Montmessin and Lefèvre, 2013 [99]). These measurements were performed by stellar occultation at night, when ozone has a long photochemical lifetime and can be reasonably assumed to be horizontally uniform. The situation is different during the day, when ozone is photolyzed by solar radiation with a timescale shorter than five minutes. As in the Earth mesosphere, daytime ozone concentrations are therefore expected to be much smaller than during the night. The amplitude of the day-night difference depends on the rate at which the ozone that is lost by photolysis is reformed by the reaction of oxygen atoms with molecular oxygen. The efficiency of this three-body process decreases rapidly with altitude. Thus, the strongest day-night differences in ozone are expected in the middle and upper atmosphere of Mars. At those altitudes, this leads to clearly heterogeneous ozone concentration for an observation performed across the terminator. The classical vertical inversion methods (so-called onion-peeling) make the hypothesis that the atmospheric composition is spherically symmetric, which fails in this case.

Figure 10 shows the vertical distribution of ozone as modeled by the photochemistry-coupled Mars LMD GCM. Here the results have been calculated with the one-dimensional version of the GCM to acquire a fine description of the ozone variation with solar zenith angle around the terminator. We have included in the figure

three lines-of-sight of a SPICAM solar occultation observation (the three lines of crosses) illustrating the path integrated during the observation. Notice that this type of inertial pointing is not within the TGO nominal solar occultation modes, although it could be performed. Figure 10 demonstrates the clear deviation of the atmosphere from the spherical symmetry due to the day-night gradient mentioned above, and the way solar occultations probe very different ozone concentrations along the line of sight.

In such a case, when comparing solar occultation observations to a model, the most straightforward method is to extract from the model the slant profiles calculated along the observational lines-of-sight, which ensures that the quantities are comparable since they have been acquired in the same way. If local vertical profiles are to be compared, the hypothesis of the spherical symmetry in the inversion method would need to be circumvented by accounting for the gradients in the atmosphere around the terminator, at least for the photochemically active species (i.e., ozone), but in the optimal case also for the full atmospheric structure.

*Aerosols* Small particles seem to be frequent at high altitudes. Particles of effective radius close to about  $1 \mu\text{m}$  have been observed by the VIRTIS and SPICAV/SOIR instruments in the Venus upper mesosphere up to 90 km during nighttime and twilight (Wilquet et al., 2009 [136], deKok et al., 2011 [26]) and scattering during daytime was observed at  $4.7 \mu\text{m}$  to be much stronger than the non-LTE fluorescence of CO up to 100 km tangent heights (Gilli et al., 2015 [50]). Using Venus as a guide, the upper limit in atmospheric pressure where scattering can be observed would correspond in the Martian atmosphere to the vertical region around 60 km. In Mars, dust detached layers with similar particle sizes have been observed with TES and MCS up to 40 km in the tropical region (Guzewich et al., 2013 [58]; Heavens et al., 2014 [60]), with TES limb data during dust storms up to 60 km (Clancy et al., 2010 [21]), and with TES up to 65 km, forming what has been named “upper dust maximum” (UDM), centered at 45-65km during daytime in the summer season in the Northern hemisphere (Guzewich et al., 2013 [58]). Also mesoscale simulations of energetic convection within dust storms suggest effective injection of particles up to 50 km (Spiga et al., 2013 [120]). The expected decrease of particles size with altitude grants the abundance of smaller particles up to much higher in Mars. Indeed there are several direct detections of aerosols at mesospheric altitudes, precisely with solar occultations in the UV with SPICAM/Mars Express (Määttä et al., 2013 [86]). They found frequent high aerosols layers between 55-70 km, even at 90 km altitude, with typical vertical extensions between 10 and 20 km, although apparently not reaching the uppermost mesosphere 100–120 km. The mesospheric aerosol layers seemed to be located at higher altitudes in the Southern hemisphere. These aerosols seemed to be associated to a large dust content at lower altitudes, during global dust storms, which possibly lofted particles up to those heights for an extended period of time, but very often they had the form of detached layers of shorter duration, outside large dust loading in the lower atmosphere.

The separation of dust and ice aerosols is another important goal that may be achieved combining UV and IR channels (UVIS and SO/MIR) during solar occultation. The above mentioned study of the SPICAM solar occultation measurements in the UV (Määttä et al., 2013 [86]) did not resolve the nature of the aerosol layers studied but suggested that many of the high altitude aerosols

might more likely be formed by water condensation than lifting of dust particles. The use of three solar occultation channels ranging from the UV to the IR has been exploited in the case of Venus to detect and retrieve distinct particles populations of three different radius (Wilquet et al., 2009 [136]). Further, the combination of particle radius and optical thickness variations within a detached aerosol layer could discriminate between dust and ice particles (Montmessin et al., 2006 [100]; Määttä et al., 2013 [86]). An interesting result from the combination of SPICAM UV and IR solar occultations during the Northern winter, obtained by Fedorova et al. (2014) [36], is the identification of a bi-modal distribution of particles on Mars at tropospheric altitudes (10-40 km). The coarser mode, with particle radius near 1  $\mu\text{m}$  was consistent with many previous atmospheric dust observations, and seemed to contain both dust and H<sub>2</sub>O ice particles, with 0.7 and 1.2  $\mu\text{m}$  radii, respectively. But their UV data were essential to identify the fine mode, with radius smaller than 0.1  $\mu\text{m}$  and reaching altitudes up to about 60-70 km in such a data sample.

In summary, the UVIS channel may extend significantly the upper atmospheric dataset of aerosols, clarifying the population and variability of small particles during periods of large dust storms and other episodes, and if combined with a concomitant IR sounding and microphysical models, clarify the nature of the aerosol layers.

### 3.2 Nadir mapping

#### 3.2.1 Infrared mapping with LNO and TIRVIM

The recent exploitation of non-LTE nadir data from VIRTIS/Venus Express by Peralta et al. (2016) [107] shows that it is possible to map the upper atmosphere not only with the classical limb sounding but also in nadir geometry, if the signal is sufficiently optically thick. This is the case of the strongest CO<sub>2</sub> band in the IR, the 4.3  $\mu\text{m}$  band system, in the case of Mars and Venus. Figure 11 shows the map of thermospheric temperatures obtained on Venus, combining very sparse data from VIRTIS during the Venus Express mission. The altitude range sampled is wide, between 100 and 150 km, and the temperatures show a global view not far from model expectations (examined at the same altitudes), except for a systematic cold bias compared to the simulations. No similar maps exist on Mars and ACS offers an opportunity for a routine mapping of thermospheric temperatures from a proper analysis of this signal.

We explored the possibility of similar sounding at other wavelengths, but the situation is not as good as in the 4.3  $\mu\text{m}$  band. Figure 12 shows the calculations for the CO<sub>2</sub> 2.7  $\mu\text{m}$  band system in a nadir geometry, as observed by the NOMAD LNO channel. This CO<sub>2</sub> band might be the second best candidate for such a mapping. The non-LTE enhancement is significant, compared to the LTE calculations, but the emission, even after spectral summation of the complete band, is about two orders of magnitude lower than the expected noise level (Table 1). Averaging of large amount of data may build up a signal but at the expense of temporal resolution. This is not a big issue in Venus, whose thermospheric structure seems more linked to the local time, but it is a serious difficulty for Mars, whose upper

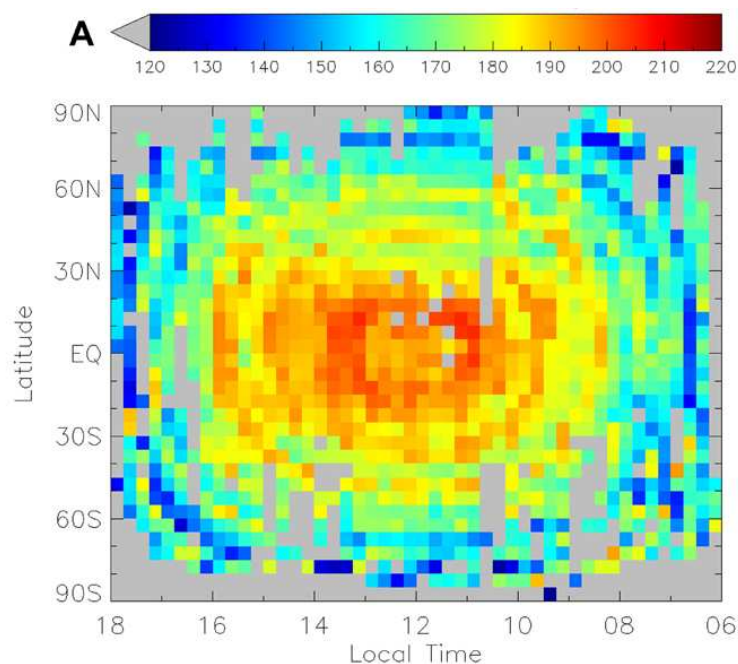


**Fig. 11** Map of Dayside thermospheric temperatures in Venus retrieved from nadir observations of the non-LTE  $4.3 \mu\text{m}$  emission by VIRTIS-H/Venus Express. After Peralta et al., 2016 [107]

atmosphere seems to be much more dynamic and variable (Piccialli et al., 2016 [108]).

### 3.2.2 Ultraviolet mapping with UVIS

The continuous UV mapping in nadir will supply a useful dataset to study airglow. The nightglow signals will be weaker than the limb components and than solar occultation detections but the accumulation of data may reveal the emissions and permit analysis of the spatial and temporal variations. One notable example is the NO nightglow, detected in the limb but not in nadir by SPICAM (Bertaux et al., 2005 [5]). This is an emission of large interest as it is associated to downwelling of atomic species ( $\text{O}^3\text{P}$  and  $\text{N}^4\text{S}$ ) from the global interhemispheric circulation during solstices (Bertaux et al., 2005[5], Stiepen et al., 2015 [125]). However, there are discrepancies between models and simulations at equatorial latitudes, where such emissions are expected to be much weaker (Gagné et al., 2013 [42]). In addition, there is a remarkable variability observed with SPICAM in the peak emission, which seems to be located between 70 and 85 km altitude but does not show any clear correlation with latitude, local time, magnetic field, or solar activity (Cox et al., 2008 [25]). Recently, nadir observations with IUVS on board MAVEN were combined into quasi-global maps of the NO nightglow revealing an unexpectedly complex structure (Stiepen et al., 2017 [126]). In addition to inhomogeneous brightening near the limb, a general intensification is observed surrounding the

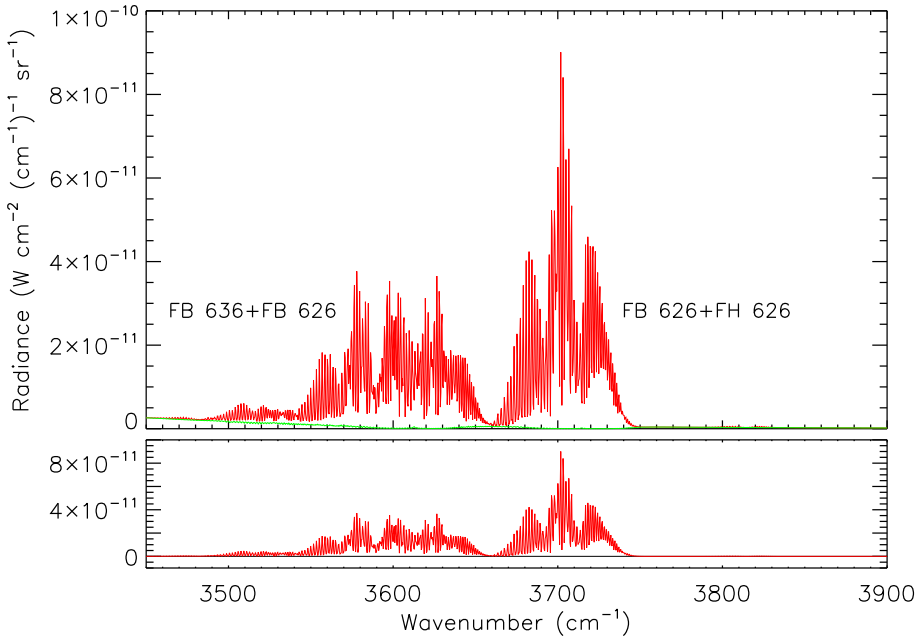


**Fig. 12** Simulation of the near-IR emission level in the center of the intense  $2.7 \mu\text{m}$  bands of  $\text{CO}_2$  during a nadir observation. Red lines: non-LTE daytime emission; green line: LTE calculation. *Bottom panel: difference between the non-LTE and the LTE spectra.*

winter pole. Streaks and spots extending toward lower latitudes suggest the presence of irregularities in the wind circulation pattern. Regarding dayglow emissions above  $200 \text{ nm}$ , these are surely very hard to detect at the nadir due to the strong signal from scattered solar radiation. The best chance to study them would be at the limb (see below).

## 4 Additional capabilities

### 4.1 TGO Aerobraking Phase

Spacecraft aerobraking maneuvers have traditionally been exploited for in-situ sounding at very high altitudes in an atmosphere. Accelerometer data during spacecraft deceleration by atmospheric drag can directly supply along-track densities, and infer vertical profiles of densities and temperatures with the help of model assumptions or hydrostatic approximation (Müller-Wodarg et al., 2016 [102]). In Mars, aerobraking has been performed during three NASA orbiters, Mars Global Surveyor, Mars Odyssey and Mars Reconnaissance Orbiter (Keating et al., 1998 [67], Withers et al., 2003 [140], Wang et al., 2006 [135], Bougher et al., 2006 [8], Moudden et al., 2010 [101]), and has supplied unique insights into the thermospheric dynamics and the links between lower and upper atmospheric regions (see Zurek et al., 2015 [147], Bougher et. al, 2017 [9], and references therein). Also, although MAVEN did not use aerobraking, it does detect atmospheric drag during

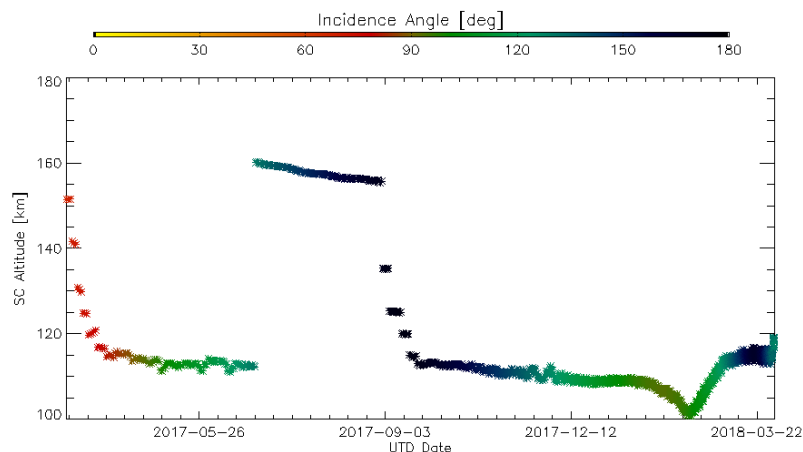


**Fig. 13** Expected evolution of the periapsis' altitude during a preliminary version of the TGO aerobraking period (see text). The colors indicate the solar zenith angle at the periapsis location, as indicated in the top scale; values above  $90^\circ$  normally correspond to nighttime.

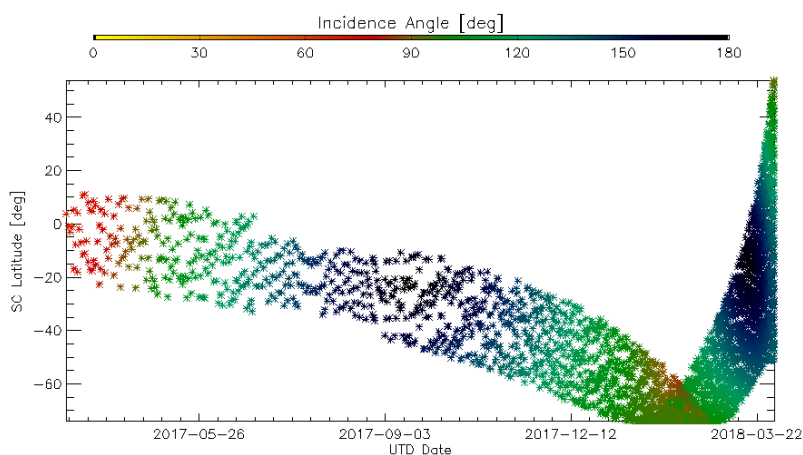


**Fig. 14** Expected evolution of the periapsis' latitude during the whole aerobraking period. As in 13 the colors indicate the solar zenith angle. The upper and lower lines show the locations where the spacecraft crosses (enters below) the 200 km reference altitude.

its orbit, specially during the deep dips into the lower thermosphere, which need to be exploited (Jakosky et al., 2015 [63], Bougher et. al, 2015 [7], Zurek et al., 2015 [147], Zurek et al., 2017 [146]). ESA, on the other hand, has performed only one aerobraking campaign, during the last phase of the Venus Express mission. These operations permitted successful retrievals of density profiles which revealed wave phenomena in polar regions (Müller-Wodarg et al., 2016 [102]) and permitted comparisons with atmospheric reference models (Bruinsma et al., 2015 [13]).

The aerobraking phase of Exomars TGO will supply an additional source of information on the still highly incomplete dataset of in-situ thermospheric densities and temperatures available to date. A large interest in the TGO dataset comes

from the combination of three factors: a wide latitudinal coverage, an extended investigation in time, and a focus on the lower thermospheric altitudes. Starting with the last one, the expected altitude range of the periapsis is [100-120] km, with some seasons at higher altitudes [150-160km], as shown in Figure 13. This is a prediction based on a preliminary estimate of the aerobraking period, extending from Jan-Nov 2017, available at the time of writing this article, and valid for us to illustrate some aspects. It will obviously depend also on the performance of the aerobraking which will be monitored on a daily basis. According to this prediction, the latitude range that could be explored during the aerobraking phase in the TGO's nearly-polar orbit goes up to  $74^\circ$  S, as shown in Figure 14. The aerobraking phase will be executed during a very extended and continuous period of time, of at least up to 9 months, covering a seasonal range  $L_s \approx 300^\circ - 90^\circ$ . As Figure 14 shows, in the first months it will probe the dayside of the planet, then move toward the dark side as the orbital period gets shorter. The part of the orbit when the spacecraft will be below 200km altitude will cover around 40 deg in latitude, until TGO orbit achieves its final circular shape at 400 km above the planet's surface. It will have a periodicity of 1 Martian day (sol) at the beginning and 2 h at the end of the aerobraking experiment.

One of the open problems whose study could benefit from the TGO aerobraking data is the propagation of gravity waves. Previous analysis using extended aerobraking datasets from MGS and Mars Odyssey suggest that such a propagation is possible up to the lower thermosphere, and might be filtered by tidal activity (Withers et al., 2006 [139]). Also non-migrating tides were detected in the aerobraking data (Wang et al., 2006 [135], Fritts et al., 2006 [41]), together with smaller scale perturbations without a clear oscillatory shape and which remain unexplained. The extended aerobraking during both day and night, including high southern latitudes, should supply new insights into these dynamical phenomena.

The combination of the aerobraking results and of the regular solar occultation data from NOMAD and ACS later in the mission also offers interesting opportunities; in particular, combining total density from aerobraking and  $\text{CO}_2$  densities from solar occultation can yield constraints on  $\text{CO}_2$  mixing ratios at thermospheric altitudes, as has recently been exploited for Venus (Limaye et al., 2017 [78]).

#### 4.2 Limb emissions off-the-terminator

We mentioned above the two major pointing modes of NOMAD and ACS, i.e., solar occultation and nadir mapping. However, there exists the possibility to perform also limb pointing with the LNO channel given its flip mirror (Neefs et al., 2015 [105]), and similarly, it is possible to perform limb observations with the TIRVIM and NIR channels by moving the nadir boresight (Korablev et al., 2017 [72]). The UVIS channel could also be operative in a limb viewing mode, co-aligned with the LNO signal. We describe four possible TGO configurations to perform a limb sounding off-the-terminator (LSoffT, in short), considering the NOMAD and ACS optical layouts.

- *LSoffT #1. Limb pointing using NOMAD flip mirror.* During regular nadir mapping, the NOMAD LNO slit is oriented across-track and its pointing could be changed to a limb pointing using the on-board flip mirror. Consequently the

slit size projected on the limb would be a 2 x 67 km oriented vertically (perpendicular to the limb) and centered at an altitude of about 67 km above the ground at the tangent, i.e., viewing altitudes between 35 and 110 km. Binning of the “spatial pixels” is possible, which will enhance the limb detection. In this configuration only the NOMAD LNO and UVIS channels would perform a limb observation, not the ACS channels.

- *LSoffT #2. Inertial limb scan.* If possible, this will be an emulation of a solar occultation sequence but off-the-terminator, i.e., the spacecraft maintains a fixed attitude (in the solar system’s reference frame), but is not pointing to the Sun. The NOMAD and ACS fields of view move across the limb due to the spacecraft’s orbital motion, effecting a limb scan. Signals from the SO, UVIS and MIR channels would be available, but the SO should be replaced by the LNO to improve sensitivity. Both the dayside and the nightside of the planet could be explored. The LNO slit would be perpendicular to the limb; this is not the ideal configuration to maximize the detection of weak emissions but it has the advantage of performing a nearly simultaneous sampling of the emissions over a wide range of altitudes (centered at 67 km if exactly perpendicular). The NIR channel can also be used in this configuration, in this case, its orientation is nearly perpendicular to the LNO slit, i.e., well positioned for spatial addition to increase detectability.
- *LSoffT #3. Nadir boresight slew.* By rotating the spacecraft around its along-track (Z) axis the boresight (-Y) axis would perform an effective limb sounding, with all NOMAD and ACS instruments operating in their regular “nadir mode”. Simultaneous signals from LNO, UVIS, NIR and TIRVIM would be available in this configuration. Attention should be given to the likely reduced pointing accuracy during such a slew maneuver, and the large fields of view of some of these channels (we will discuss these below).
- *LSoffT #4. Fixed limb tracking.* After the simple inertial limb scan (LSoffT#2) and/or the nadir boresight slew (LSoffT#3) have been tried, a next step would be to position the spectrometer slit across the limb to perform a fixed limb tracking, that is to keep the slit pointed at a fixed tangent altitude above the planet as the spacecraft moves through its orbit. This allows a truly 2D map of limb emissions to be built up, and permits also long integration of faint sources. A similar strategy was used on Venus Express to search for oxygen airglow (Migliorini et al., 2013 [97]). Both, the solar occultation channels (as in LSoffT#2) or the more sensitive nadir ports (as in LSoffT#3) could be used. Notice that LSoffT#1 also represents a limb tracking but at the fixed tangent altitude of 67 km above the surface and using only two NOMAD channels.

These non-standard observational configurations would add new ways of exploiting the TGO science, and therefore, we recommend its use during short upper atmosphere campaigns. We mention next several of the scientific goals inherent to these LSoffT modes which, if confirmed with observations, would represent valuable and added science. Some of them are of a general character and require specific examination, but all merit their execution and testing. The first one is the building of vertical profiles of minor species and dust outside the very peculiar region at the day/night terminator. Also, these observations shall permit to complete the daily

cycle of minor species (chemistry & dynamics) outside the specific local times of the terminator at each latitude. Specific emission from solar fluorescence and airglow data would permit to study the upper atmosphere physics behind them, and perhaps to derive information about the thermal structure in the vertical. After detection of specific areas on the planet where trace gases are found, a vertical sounding capability above such areas would be of large interest, if their emission in a limb geometry permit to gain insight into their vertical distribution. These observations would also extend in time the current database of Mars limb observations to date (OMEGA, PFS and SPICAM on Mars Express, TES on MGS, and MCS and CRISM on board MRO).

In addition, there could be defined a number of moments during the mission for specific new targets which shall require these observing modes. Four examples are (i) the search for very high altitude clouds, airglow and aurora phenomena, (ii) the investigation of the thermal structure in very-high-latitude regions and its daily cycle, (iii) **2D mapping of emissions and densities using the limb-tracking modes, which could depict the propagation of gravity waves**, and (iv) broad spectroscopic searches from the UV to the IR at these altitudes, opening a window for serendipity science. Some of these are expanded in more detail next. In summary, we anticipate that both NOMAD & ACS will increase their scientific impact thanks to these LSoFT observation modes.

#### 4.2.1 Nightglow

*Mars aurora* The Martian aurora, observed for the first time with SPICAM/MEx (Bertaux et al., 2005 [6]), was sporadic, associated to magnetic anomalies in the crust, and peaked at about 135 km. Later, a different kind of aurora, diffuse, quasi-global and down to 60 km altitude, was observed with IUVS/MAVEN during periods of strong solar activity (Schneider et al., 2015 [115]). Martian auroras have triggered renewed interest in the Martian upper atmospheric emissions as probes of the thermospheric structure and as validation tools for models (Gagné et al., 2013 [42]; Gerard et al, 2015 [47]; Soret et al, 2016 [119]).

The SPICAM observations show prominent UV emissions from the CO ( $a^3\Pi - X^1\Sigma$ ) Cameron Bands (190-270 nm), the CO<sub>2</sub>+ doublet around 289 nm, and the atomic oxygen 297.2 nm trans-auroral line. Figure 15 shows the vertical intensity profiles from the CO Cameron and the CO<sub>2</sub>+ doublet observed with SPICAM and studied by Soret et al., 2016 [119], who could reproduce the altitudes of the auroral emissions with a Monte-Carlo model of electron transport in the Martian thermosphere. The diffuse aurora shows similar spectral features but with lower intensity levels and peak altitudes (Schneider et al., 2015 [115]).

UVIS should combine nadir and limb emission observations to study the intensity and the spatial distribution of the auroral emissions, with attention to the residual magnetic field regions and to strong solar events. Recently, Lilensten et al. (2015) [77] suggested that during strong solar events there could be auroral emissions in the visible, possibly localized as well, including the red and green lines of atomic oxygen and the CO<sub>2</sub>+ Fox-Duffenbach-Barker (FDB) bands in the blue-visible spectral region. The UVIS channel offers possibilities to detect such events. A specific limb inertial mode in the nightside hemisphere during such solar conditions would be most adequate for such a study.

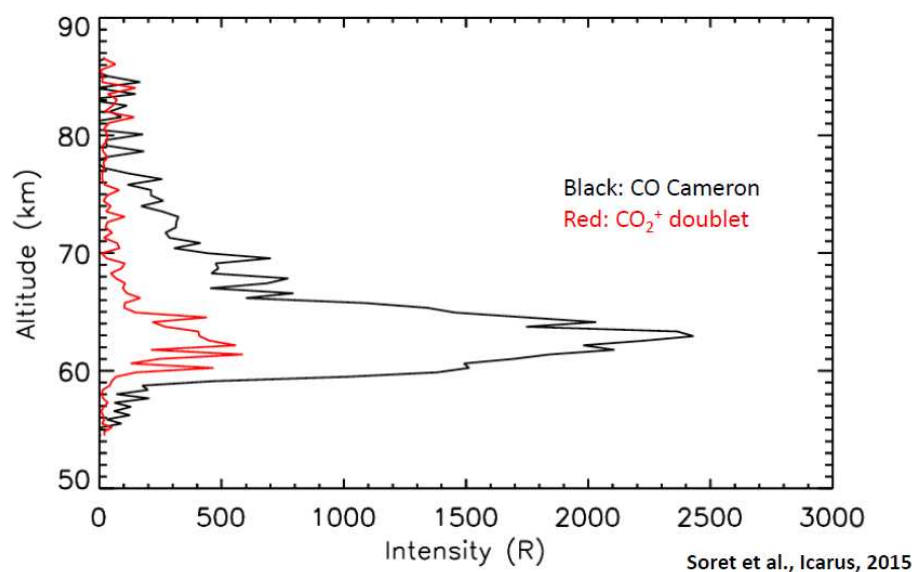


**Fig. 15** Vertical profiles of UV auroral emission in Mars, observed with SPICAM. After Soret et al., 2016 [119], with permission. Notice that these are apparent limb profiles, before correction for the non spherical symmetry of the discrete aurora; the actual peak emissions occur around 120-130 km.

*O<sub>2</sub> IR Atmospheric bands at 1.27  $\mu\text{m}$*  The O<sub>2</sub> IR airglow at 1.27  $\mu\text{m}$  has been extensively studied in Venus using ground based telescopes and spectral images at the nadir and limb obtained with the VIRTIS spectral imager on board Venus Express. Its detection in the Mars nightglow spectrum is much more recent. The first detection was made with the OMEGA instrument on board Mars Express (Bertaux et al., 2012 [4]). This emission was further investigated and its seasonal variations were characterized with CRISM on board the MRO satellite (Clancy et al., 2012 [17]) and SPICAM IR on Mars Express (Fedorova et al., 2012 [34]). Detections were made close to the southern and northern poles during polar night. This nightglow layer is produced by three-body recombination at 40-50 km of oxygen atoms produced on the dayside by CO<sub>2</sub> dissociation and transported to the polar dark regions by the global circulation. The intensity observed by CRISM at the limb reaches about 14 Megarayleighs (MR), a brightness that should be measurable with the NIR/ACS channel. Comparisons with GCM predictions (Gagné et al., 2013 [42]) indicate that the model underestimates the high latitude O<sub>2</sub> airglow brightness by a significant margin. Although high latitude measurements will be limited by the TGO orbital inclination, the mid-latitude brightness near equinox may be observed and the O density derived from these observations. Unfortunately, the altitude range where this derivation is possible does not cover the upper mesosphere and lower thermosphere. This is the region where the strongest CO<sub>2</sub> emissions at 15- $\mu\text{m}$  occur and depend most on the collisional exchanges between atomic oxygen and CO<sub>2</sub>; and this is the process which together with the EUV heating mentioned in section 2 dominates the energy balance of the Mars upper atmosphere (López-Puertas and López-Valverde, 1995 [79]).

*NO UV nighttime emission* Detected with SPICAM between 60 and 90 km altitude (Leblanc et al., 2006, [74], Stiepen et al., 2015 [125]), and a variable intensity which can reach about 10 kR for the total  $\delta$  and  $\gamma$  bands, these emissions are possibly detectable with UVIS. Since they seem to be largely related to summer-to-winter interhemispheric circulation and downwelling in the night side, their emissions seem to be stronger at high winter latitudes. However, the detection at low latitudes is also of large interest, as it is a puzzle for global models, which can not explain such observations (Stiepen et al., 2017 [126]).

*NO nightglow in the near-IR* A weak band of NO between two electronic states ( $C(0) \rightarrow A(0)$ ), and whose Q-branch is centered at  $1.244 \mu\text{m}$ , has been sporadically observed on the Venus nightglow (Garcia-Muñoz et al., 2009a [44]). The upper state of the transition,  $C(0)$ , is probably excited during nighttime at high altitudes in the terrestrial planets' atmospheres by recombination of nitrogen and oxygen atoms. The peak tangent altitude in Venus is around 110 km, whose equivalent pressure level on Mars could be 70-90 km. With a Venus limb emission around 10-30 kR, this is probably too weak for detection in Mars with NIR. However, the operation modes LSoft # 2-4 are optimized to perform such a search. One of the difficulties for its detection is the close and stronger  $O_2 a(0) \rightarrow X(0)$  emission band at  $1.27 \mu\text{m}$  and the OH (7-4) Meinel band at  $1.21 \mu\text{m}$ . In case of detection, other two associated transitions from the two excited states to the ground ( $C \rightarrow X$  and  $A \rightarrow X$ ) between 190 and 280 nm, mentioned above, could be visible by UVIS. Indeed they seem to occur at about the same altitude range, **and according to the Venus case they could be about a factor 2 stronger** (Garcia-Muñoz et al., 2009a [44]).

*Atomic oxygen green line emission* Since its discovery on Venus by Slinger et al. (2001) [116], the green line has sporadically been observed on Venus during times of enhanced solar activity (Gray et al., 2014 [56]). However, the brightness was low, on the order of 10 to 170 Rayleigh, and that should be an upper limit for Mars as well. The green line is a challenge for UVIS, which should look for its limb emission during active sun conditions. NOMAD-UVIS is the only instrument covering the near-UV and visible ranges, and is specially suited to tackle the task of detecting this line (Lilensten et al., 2015 [77]).

*O<sub>2</sub> bands in the UV and visible* In the near UV and the visible range, 260-450 nm approximately, the  $O_2$  Herzberg II bands ( $c^1 \sum_u \rightarrow X^3 \sum_g$ ) are an exciting (and difficult) challenge for UVIS, and we mention them here as a possibility. They were below the detection capability of Mars 5 but models estimate a limb emission in the order of a few kR (Gagné et al., 2012 [43]). Its intensity should be larger in the nightside winter hemisphere and its detection with UVIS might lead to the derivation of atomic oxygen abundances in its emission layer, which could possibly be around 50 km, from comparison with the Venus emission layer (Gagné et al., 2012 [43]). Other emission bands of  $O_2$  in the near UV and in the visible ranges, like the Herzberg I and the Chamberlain systems, are about an order of magnitude weaker in the Venus mesosphere, and their detection in Mars is even more difficult (Garcia-Muñoz et al., 2009 [45]).

*OH Meinel bands* Several IR transitions should be explored. The emissions with  $\Delta v=1$ , around  $3 \mu\text{m}$ , were observed on Venus with VIRTIS (Piccioni et al., 2008 [110], Gerard et al., 2010 [48]) and on Mars with CRISM in the polar night at tangent altitudes around 50 km (Clancy et al., 2013 [16]). The intensity of the sum of the two brightest bands, (1,0) and (2-1), is about 2 MR while the emission at  $1.45 \mu\text{m}$  from the (2-0) band reached about 200 kR. These values refer to the dark polar atmosphere which is probably the region of highest intensity according to CRISM data. These are the conditions where the LNO and NIR may detect these emissions in a limb observing geometry.

#### 4.2.2 Dayglow and fluorescent emissions

Strong daytime emissions in the UV and IR regions covered by NOMAD and ACS have been observed by SPICAM, IUVS/MAVEN and OMEGA in the limb. They offer the possibility to derive densities and temperatures at thermospheric altitudes in the dayside, from their vertical emission profiles. The large intensity of some these emissions offers good chances for TGO to detect them.

*UV dayglow* UV dayglow limb observations were measured by the Mariner missions (e.g. Stewart et al., 1992 [124]) and by SPICAM (Leblanc et al., 2006 [74]; Stiepen et al., 2015 [125]). A comprehensive pre-MAVEN review is found in Bougher et al., 2017 [9]. Recently, MAVEN IUVS UV dayglow limb observations were reported by Jain et al., 2015 [62]. In the UVIS spectral range, detected features include the CO Cameron band, the  $\text{CO}_2^+$  UV doublet and the  $\text{N}_2$  Vegard-Kapland bands. Figure 16 shows a composite dayglow spectrum built by combining those sources at their peak thermospheric tangent altitudes in order to illustrate the expected spectral locations and intensities. Thermospheric temperatures have been derived from the limb profile of some of these emissions, showing an important short-term variability. However, analysis of SPICAM and IUVS/MAVEN datasets seem to provide contradictory conclusions regarding the variability with solar activity of dayglow-derived temperatures (Stiepen et al., 2015 [125]; Jain et al., 2015 [62]). Furthermore, recent NGIMS/MAVEN neutral density-derived temperatures suggest a solar activity trend very similar to IUVS datasets (Bougher et al., 2017 [12]). UVIS limb observations would be helpful to improve the geographical and temporal coverage of the current measurements and to shed some additional light on the issue of solar variability of the temperatures at these altitudes.

The extension of the UVIS channel into the visible creates new possibilities. It makes it possible to measure the near UV-Visible  $\text{CO}_2^+$  FDB bands extending between 320 and 430 nm and the CO (d-a) triplet transitions at longer wavelengths. The presence of the FDB bands in the dayglow and the aurora was detected, but only marginally observed by previous space missions as a consequence of the limited long-wavelength cutoff of the photo-cathodes used so far in embarked spectrographs. The green line at 557.7 nm is not included in figure 14, as it is a nightglow feature, but is expected to be several times as bright as the OI 297.2 nm emission in the dayglow (Gattinger et al., 2009 [46]).

*IR non-LTE emissions by CO and  $\text{CO}_2$*  Piccialli et al., 2016 [108], described in detail the strong non-LTE fluorescence by  $\text{CO}_2$  at  $4.3 \mu\text{m}$  observed in OMEGA

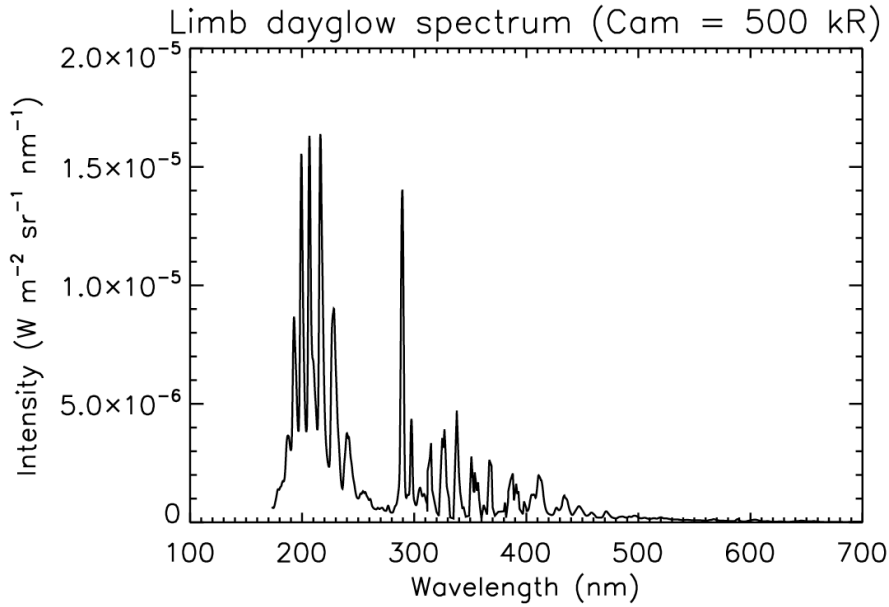


**Fig. 16** Composite dayglow spectrum at thermospheric altitudes based on Mariner, IUVS/MAVEN and laboratory measurements. The emissions include the CO Cameron bands, the CO<sub>2</sub>+ UV doublet, the OI 297.2 nm line, the CO<sub>2</sub>+ FDB bands and the CO (d-a) triplet transitions. The intensities are normalized to a Cameron band brightness of 500 kR. See text.

limb data up to the upper thermosphere, and similar limb emissions by CO<sub>2</sub> and CO have been observed with PFS (Formisano et al., 2006 [39]). These are best candidates for adding sounding capabilities to TGO in the infrared during daytime. While the 4.3  $\mu\text{m}$  emission can no doubt be detected with TIRVIM, if pointing to the limb is performed, the second strongest emission band system by CO<sub>2</sub>, that at 2.7  $\mu\text{m}$ , and suitable for the NOMAD LNO channel, has a weaker emission. Figure 17 shows a simulation at 2.7  $\mu\text{m}$  in the LNO channel using a non-LTE model [84] and a line-by-line radiative transfer model (Dudhia, 2017 [28]) and including the LNO characteristics. The NESR value of the LNO signal is a key factor; **if the value used in Figure 17 is correct, this observation would require large integration times.**

These two emissions are suitable for retrieving densities and temperatures in the Martian daylight hemisphere at mesospheric altitudes, and perhaps up to the lower thermosphere. The case of the 4.3  $\mu\text{m}$  observations with TIRVIM has the handicap of the wide field of view, but even such data can be inverted if the shape of the non-LTE emission is well characterized. Such a profile shape is well understood in theoretical terms. A similar problem with another non-LTE emission, by CO<sub>2</sub> at 10  $\mu\text{m}$  as measured with ground based telescopes, has recently been exploited to derive Martian mesospheric winds at the emission peak altitude (López-Valverde et al., 2016 [85]).

*High altitude clouds in the visible* Sanchez-Lavega et. al ([114]; see Figure 18 extracted from that work) reported peculiar images of Mars obtained by amateur

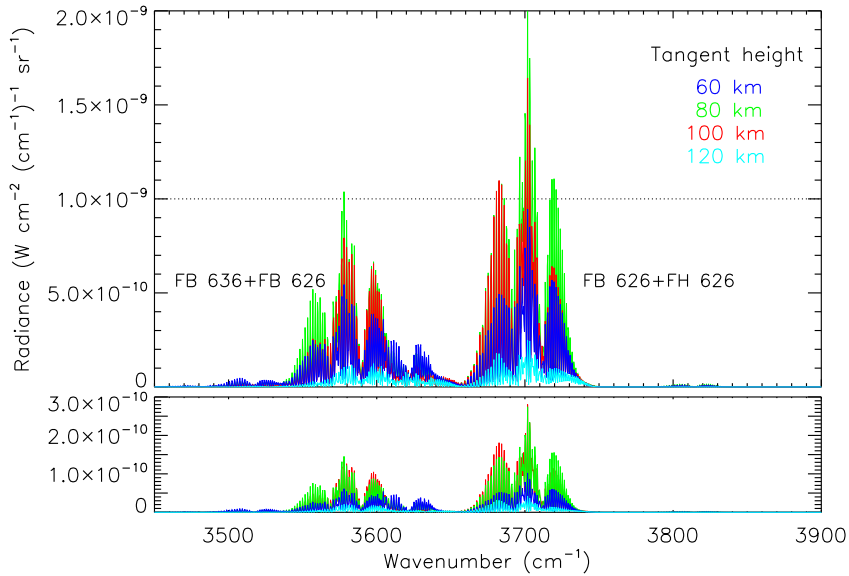


**Fig. 17** Upper panel: Simulation of the emission at  $2.7 \mu\text{m}$  in a limb geometry as measured by the NOMAD LNO channel, at four tangent altitudes and their sensitivity to the atmospheric  $\text{CO}_2$  abundance. The dotted line is the expected noise level. **Bottom panel: response to a 20% increase in the  $\text{CO}_2$  abundance.**

astronomers from small-size ground-based telescopes, showing what looked like very high altitude clouds during several days in March 2012. The reported altitude, around 200 km, is simply too high for any known condensation phenomena, and although a few tentative explanations have been proposed (Sanchez-Lavega et al., 2015 [114]; Andrews et al., 2016 [2]), all look unlikely and unsatisfactory. The issue remains open and waiting confirmation from more observations. Observations from an orbiter like TGO making profit of its wide spectral range could clarify the issue. Ideally they should be carried out in a limb geometry around the twilight and early morning hours. We suggest to combine the UV and the near IR capabilities of TGO, in particular simultaneous observations with UVIS/NOMAD and NIR/ACS during specific campaigns over the regions and times where the phenomena occurred.

Figure 19 shows another kind of high altitude clouds, this time of  $\text{H}_2\text{O}$  ice particles at mesospheric altitudes using VIRTIS on board the Rosetta spacecraft during its Mars fly-by in 2007. These images, obtained in the equatorial region at  $1.3 \mu\text{m}$  could indicate clouds located as high as 100 km due to the line-of-sight projection. This result must be looked upon with caution; SPICAM could not detect such clouds during solar occultation in the UV and IR. High altitude  $\text{H}_2\text{O}$  ice clouds are suitable for detection with the ACS/NIR channel if performing limb soundings. It has become clear the importance of the water-ice clouds in the Mars climate system; from their non-negligible impact in the radiative balance and the global circulation (Wilson et al., 2007 [138]; Wilson et al., 2014 [137], Navarro et al., 2014 [104]) to their possible role in the formation of geologically young subsurface ice deposits during certain past periods (Madeleine et al., 2014 [87]).

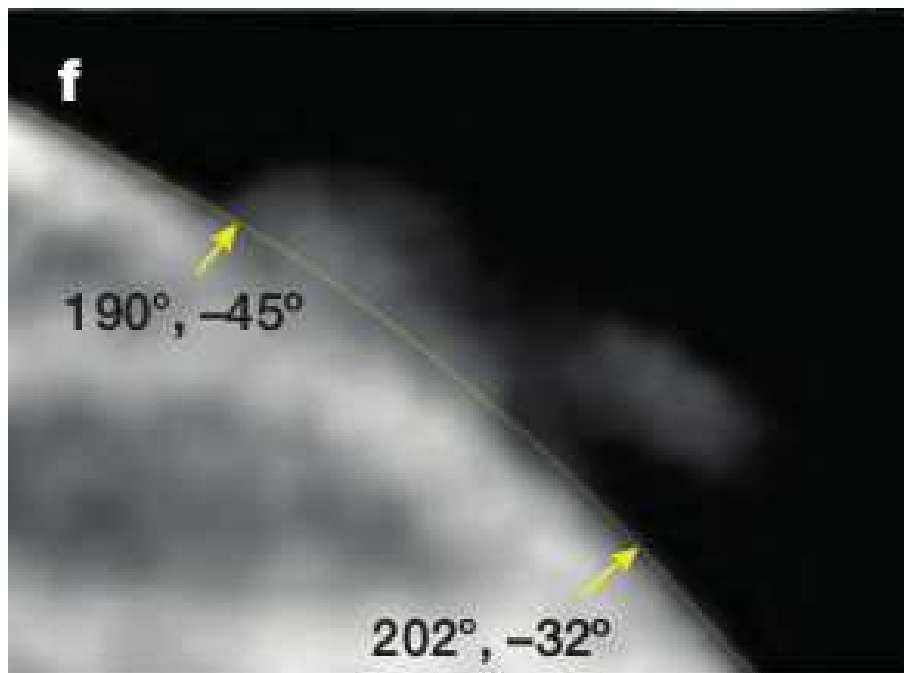


**Fig. 18** Ground-based observations of high altitude structures as reported by Sanchez-Lavega et al., 2015 [114]. Adapted from this reference with permission.

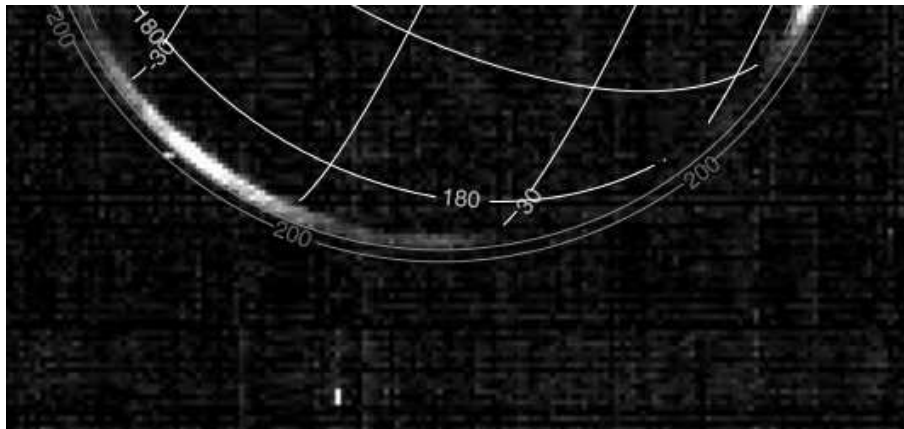


**Fig. 19** Limb detection of high-altitude H<sub>2</sub>O clouds with VIRTIS/Rosetta at 1.3 μm. The external curves indicate 100 and 200 km of altitude above the disk edge. After Coradini et al., 2010 [24].

Understanding its formation, dust scavenging capabilities, and its variability is of importance for realistic simulations of the Mars climate (Villanueva et al., 2016 [134]).

### 4.3 Expanding synergies between NOMAD and ACS

Cross-validation and complementarity of NOMAD and ACS should be exploited for an accurate upper atmospheric sounding. Although simultaneous solar occultations from SO and MIR cannot be obtained due to the boresight misalignment described earlier, intercomparison of observations performed at similar locations and times would be valuable for cross-validation. A special occultation mode but with LNO and MIR, even if performed just once, might supply also additional cross-calibration of these two important channels, which could be very useful for comparing results during their systematic nadir mapping phase, and for considering them as potential limb sounders of the upper atmosphere in possible special operation modes (LSoffT #2 and #3 scenarios, see Section 3).

In the spectral domain there is a clear complementarity between NOMAD and ACS channels, as mentioned above, and special TGO operation modes could add interesting cases to improve upon such a synergy. One example is sounding limb fluorescent IR emissions at  $2.7 \mu\text{m}$  in the LNO channel, which should correlated with similar emissions at  $4.3 \mu\text{m}$  in the TIRVIM channel. And a second one, acquiring very broad spectra, from the UV to the near-IR, combining the UVIS and NIR channels in a limb geometry should have a great potential for exploring high altitude clouds and serendipity phenomena.

### 4.4 Synergy with Mars Express, MAVEN and other projects

#### 4.4.1 Mars Express

The extension of Mars Express until the end of 2018 (<http://sci.esa.int/director-desk/58589-two-year-extensions-confirmed-for-esa-s-science-missions>) is excellent news also for the upper atmosphere regarding simultaneous observations from both European Mars missions. Mars Express instruments OMEGA, SPICAM and PFS have been extremely successful studying the upper atmosphere using both emission and absorption data (Titov et al., 2017 [130]). Mars Express offers the opportunity to perform correlated observations and cross-validation with TGO instruments, and with both the nominal observation modes and the possible additional modes discussed above. The very different orbits offer chances to complement each other in areas like daily cycles of dust and ice (Giuranna et al., 2017 [51]). Also, new tools for exploitation of Mars Express data are under development, with the goal to apply them to Exomars TGO instruments, opening the door for optimal exploitation of both datasets (<http://www.upwards-mars.eu/>). These tools include synergistic retrieval schemes **combining two spectral ranges and/or different instruments** (Robert et al., 2017 [111]), non-LTE limb retrievals for the infrared (Lopez-Valverde et al., 2016 [81]), and multiple-scattering retrieval schemes for joint extraction of gas species (water vapor, CO<sub>2</sub>, CO) and dust and ice (Mahieux et al., 2017 [89]). Once the regular operations start and the orbit is well determined, it will be straightforward to determine the orbital coincidences and to prepare correlated studies and mutual validations, from the UV to the IR.

#### 4.4.2 MAVEN

The NASA mission Mars Atmosphere and Volatile Evolution (MAVEN) is devoted to the study of the upper atmosphere of Mars, its interaction with the Sun and solar wind, and the processes resulting in atmospheric loss to space (Jakosky et al., 2015 [63]). It includes a suite of instruments that can be divided in three packages: the Particle and Fields package, including instruments for the in-situ characterization of the solar output and the composition of the solar wind, as well as the electronic density and temperature; the Imaging UV Spectrometer (IUVS), a remote sensing instrument to study the UV spectra of the planet; and the Neutral Gas and Ion Mass Spectrometer (NGIMS) to measure in-situ the composition of the neutral atmosphere and the ionosphere. An accelerometer is also on-board to determine the atmospheric density during the periapsis portion of the orbit. More details about the instruments can be found in Jakosky et al. (2015) [63] and references there in.

The MAVEN orbit has a nominal periapsis of 150 km, a period of 4.5 h, i.e. about 5 orbits per day, and an inclination of  $75^\circ$ . During selected periods lasting approximately 5 days, MAVEN conducts the so-call “deep-dips”, where the periapsis altitude is lowered to about 125 km, allowing for an in-situ characterization of the lower thermosphere of the planet.

Focusing on the characterization of the neutral upper atmosphere, MAVEN has measured temperatures using a variety of techniques: stellar occultation with the IUVS instrument (Groller et al., 2015 [57]) (altitude range 100-150 km), from the scale height of the densities measured by NGIMS (Mahaffy et al., 2015 [88]) (from 200 to 300 km), from the hydrostatic integration of NGIMS CO<sub>2</sub> and Ar over an altitude range of periapsis to about 200 km (Bougher et al., 2017 [12]), and from the scale height of the UV dayglow observed by IUVS (Jain et al., 2015 [62]; Evans et al., 2015 [32]) (from 150 to 220 km). The abundance of chemical species in the neutral upper atmosphere has been measured by NGIMS [88], including among its targets species such as CO<sub>2</sub>, Ar, CO, O, O<sub>2</sub>, N<sub>2</sub>, N and NO. Also IUVS observations have provided densities of CO<sub>2</sub>, N<sub>2</sub> and O<sub>2</sub> (Evans et al., 2015 [32]; Stevens et al., 2015 [122]; Groller et al., 2015 [57]). Information about wave activity, including tides and small scale gravity waves has also been obtained from IUVS, NGIMS and the Accelerometer (Yigit et al., 2015 [145]; England et al., 2016 [30]; Zurek et al., 2017 [146]). And very recently, a set of IUVS periapsis observations with pointing at 60-80 km tangent altitudes during the early morning showed detached layers of enhanced mid-UV solar scattering, which have been attributed to CO<sub>2</sub> mesospheric clouds, perhaps associated to temperature minima produced by non-migrating tides which could propagate even up to thermospheric altitudes (Stevens et al., 2017 [123]).

There is a significant degree of overlap between MAVEN and TGO physical products. In particular, temperature and densities of some species (carbon species CO<sub>2</sub> and CO for example) are obvious targets of both missions. We focus here on two important aspects which are complementary between the two missions: the altitude range and the local time.

- TGO solar occultations should sound the Martian atmosphere up to about 160 km, while regular MAVEN in-situ sounds down to about 150 km, although during deep-dips this lowest layer goes down to mesopause/homopause altitudes.

In addition IUUVS/MAVEN is remotely sounding the lower thermosphere, for a perfect match with TGO goals there. So, joint analysis of data from both missions will significantly extend the individual altitude ranges and provide valuable information about couplings between different atmospheric layers. The possible impact on atmospheric escape of an increased H<sub>2</sub>O abundance at mesospheric altitudes, the altitude variation of the D/H ratio, and the role of wave propagation in the thermosphere are examples of topics that can be benefited from this complementarity.

- IUUVS/MAVEN does not focus on the terminator, and will therefore supplement TGO's observations precisely there, and viceversa. Again one interesting topic to tackle by combining the two missions is the characterization of the waves propagating from the lower atmosphere, as mentioned above. Another example is the occurrence of mesospheric clouds, which are being observed in the daylight hemisphere by UVIS/MAVEN from their UV scattered solar radiation (Deighan et al., 2017 [27]). And a third example is the coordinated mapping of the UV airglow features that can be achieved, and which could be improved with the implementation of the TGO "LSoffT" modes mentioned above.

#### 4.4.3 Mars Reconnaissance Orbiter

The Mars Reconnaissance Orbiter (MRO) [Zurek and Smrekar, 2007] ([113]) continues orbiting Mars after more than 10 years of regular operations from a polar orbit 250-320 km above the surface of the planet. With an orbital period of 112 minutes and fixed local times at the equator, there will be very good coincidences with the TGO solar occultations every few weeks, and approximate coincidences twice every orbit. These can be determined more precisely once the regular TGO orbit is achieved (possibly March 2018), opening up a period of very interesting synergies.

#### *CRISM and MARCI*

The Compact Reconnaissance Imaging Spectral Mapper (CRISM) (Murchie et al., 2007 [103]) is a visible-nearIR ( $\lambda = 0.4 - 4\mu m$ ) high spatial (pixel size in the nadir direction  $\sim 15-20$  m), moderate spectral ( $\Delta\lambda = 7-15$  nm) resolution imaging spectrometer on MRO. Although the primary role for CRISM is mineralogical surface mapping, its spectral range and resolution have supported a number of key atmospheric measurements in nadir and limb (2-3 orbits every  $\sim 3$  months) observing modes. Atmospheric objectives have included column measurements of water vapor and CO (Smith et al., 2009 [117]), dust and ice (H<sub>2</sub>O and CO<sub>2</sub>) aerosol physical properties Wolff et al., 2009 [144]; Clancy et al., 2015 [18]), polar OH and O<sub>2</sub> nightglow [Clancy et al., 2013, 2012 [17] [16]), and O<sub>2</sub> dayglow/inferred water vapor profiles retrievals (Clancy et al., 2017 [16]). CRISM inferred water vapor vertical profiles over 10-60 km altitudes have been compared to Mars Express SPICAM solar occultation profile measurements (Maltagliati et al., 2013 [94]), and would provide the most extensive existing Mars water vapor profile data set for climatological cross comparisons with TGO NOMAD and ACS key water profiling observations (Figure 20). CRISM visible-near IR dust and ice aerosol physical property measurements (Wolff et al., 2009 [144]) also provide full spectral coverage

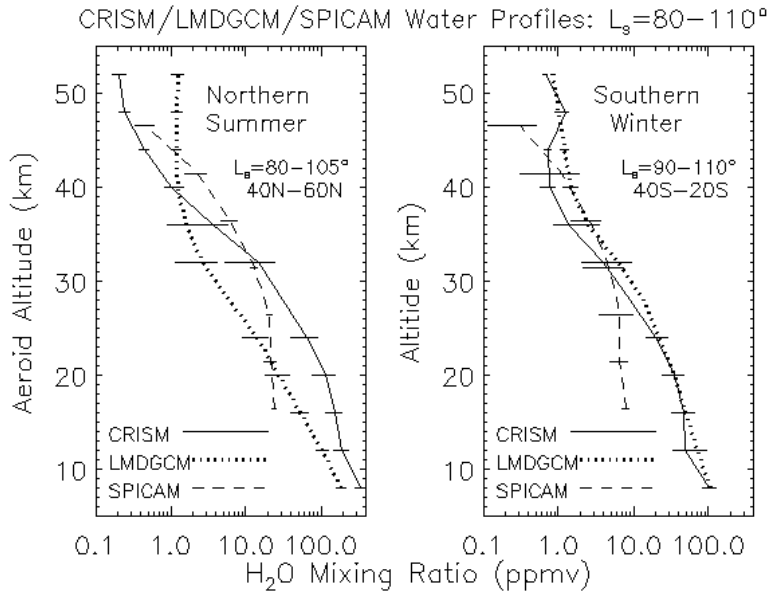


**Fig. 20** Binned average vertical water vapor profiles over the northern summer season ( $L_s=80-110$ ) are compared for southern (right,  $40S-20S$ ) and northern (left,  $40N-60N$ ) latitude ranges, as inferred from CRISM  $O_2$  airglow (solid), LMD GCM simulations (Navarro et al., 2014 [104], dotted), and SPICAM solar occultations (dashed). Figure reproduced from Clancy et al., 2017 [19].

comparisons with the NOMAD and ACS narrow band nearIR measurements, and over the 400-700 nm wavelength measurements of the NOMAD UVIS instrument.

The Mars Color Imager (MARCI) is a wide-angle camera on MRO designed to obtain daily global image maps of Mars, at a local time of 3pm, in two UV (265nm, 320nm) and 5 visible (420-750 nm) filter channels (Malin et al., 2008 [93]). MARCI UV global imaging has supported daily global mapping retrievals for column  $O_3$  (Clancy et al., 2016 [20]) and ice cloud optical depths (Wolff et al., 2013 [142]) over 6 Mars years (2006-2017) and continuing. MARCI daily global maps of Mars  $O_3$  columns provide sensitive high latitude and aphelion measurements with unprecedented spatial and temporal coverage, but do not constrain low-to-mid latitude  $O_3$  columns during perihelion periods due to dust contamination issues (Clancy et al., 2016 [20]). Nevertheless, they yield extraordinary NOMAD UVIS  $O_3$  measurement comparison opportunities due to their contemporaneous global and daily coverage. Similarly, MARCI 320 nm cloud optical depth retrievals (Wolff et al., 2013 [142]) provide exceptional contemporaneous cloud measurement determinations with respect to NOMAD UVIS brightness, as well as dust UV optical properties derived from MARCI UV observations during periods of high dust loading (Wolff et al., 2010 [143]).

#### *Mars Climate Sounder*

The Mars Climate Sounder (MCS) (McCleese et al., 2007 [95]) is a passive infrared radiometer on MRO which views the martian atmosphere in limb, nadir, and off-nadir geometries. It has five mid-infrared (12 to 22  $\mu\text{m}$ ), three far infrared (32 to 42  $\mu\text{m}$ ), and one broadband visible/near-infrared (0.3 to 3  $\mu\text{m}$ ) channels. Profile retrievals of temperature, dust extinction, and water ice extinction are performed operationally for all limb measurements [Kleinböhl et al., 2009, 2011] ([69, 70]) and cover a vertical range from near the surface to 80-90 km altitude. MCS obtains daily global (pole-to-pole) coverage at six fixed local times (Kleinböhl et al., 2013 [68]). MCS is also designed to observe the atmosphere in nearly coincident, simultaneous limb observations with those provided by other limb viewing instruments. Using its nearly hemispheric scanning capability, MCS currently makes such coincident measurements regularly with the MRO radio science investigation and CRISM limb-scans to provide complementary temperature, dust, and  $\text{CO}_2$  and water ice cloud measurements, as well as providing essential measurement validation. In addition, MCS performs measurement campaigns in order to obtain coordinated measurements with the atmospheric instruments on the Mars Science Laboratory and with stellar occultation observations by the UVIS instrument on-board MAVEN as well as with MAVEN deep dip campaigns, in which the MAVEN periapsis is lowered in order to probe the lower parts of the upper atmosphere. During TGO's initial payload checkout orbits, MCS demonstrated this capacity in cooperative observations with NOMAD and will do so with ACS and NOMAD when TGO begins science operations. Figure 21 shows temperature, dust, and water ice profiles measured by MCS at three local times in the afternoon. The measurements were obtained in the same region and about 30 minutes after NOMAD performed test measurements from TGO on November 26, 2016. Temperature profiles were retrieved throughout the lower and middle atmosphere up to an altitude of 80-90 km. Note that surface temperatures around 280 K were also retrieved from the MCS measurements. The dust profiles are typical for the season ( $L_s=269$ ) with a steep fall-off between 30-40 km altitude. They are overlaid by water ice layers around 40 km altitude at local times around 13 h and 16 h.

MCS limb measurements will have significant vertical overlap with TGO solar occultation measurement from which density and in turn temperature can be retrieved. This will allow the construction of temperature profiles reaching from the upper atmosphere to the surface. Additionally, the global coverage of MCS will provide atmospheric context and complementary coverage of local time for the interpretation of TGO measurements. This will enable the study of the propagation of tides and gravity waves into the upper atmosphere [e.g. Lee et al., 2009, Kleinböhl et al., 2013] ([68, 76]), as well as the influence of dust storms on the upper atmosphere due to their early detection and monitoring by MCS (e.g. Kass et al., 2016 [66]). MCS has identified mesospheric dust layers (Heavens et al., 2015 [59]) as well as water ice clouds (e.g. Kleinböhl et al., 2017 [71]) that reach altitudes of 60-70 km. Coordinated measurements with TGO will allow the derivation of aerosol properties and provide insight into the formation processes of water ice clouds and the transport processes controlling water vapor and dust at mesospheric altitudes.

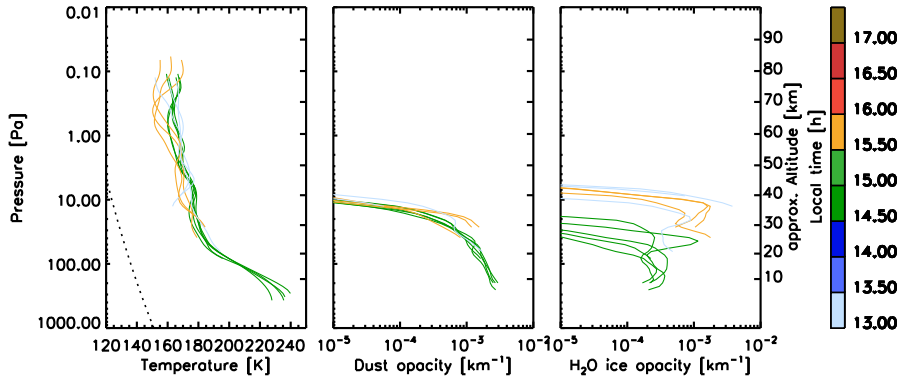


**Fig. 21** Temperature (left), dust opacity (reported at 463 cm<sup>-1</sup>, center) and water ice opacity (reported at 843 cm<sup>-1</sup>, right) as measured by MCS between 10°S and 10°N on November 26, 2016 in coordination with NOMAD measurements from TGO. The dotted line in the left panel is the CO<sub>2</sub> condensation temperature.

#### 4.4.4 James Webb Space Telescope

The James Webb Space Telescope, expected to be launched in 2018, is suitable for observing Mars with some of its instruments, particularly with NIRSPEC, and this offers opportunities for correlative measurements with TGO instruments. NIRSPEC will cover the 0.75  $\mu\text{m}$  spectral region with a resolving power around 2700, and twice this value in the 1.0-1.25  $\mu\text{m}$  window. Its viewpoint, from the second SunEarth Lagrange point (L2) permits to observe the full disc. The scientific opportunities for Mars have been recently reviewed by Villanueva et al. (2016) [134] and include the exploration of upper atmospheric temperatures using the 4.3  $\mu\text{m}$  band. This therefore offers chances to perform correlative observations with the ACS TIRVIM channel in the same spectral region, but with a completely different spatial resolution.

Figure 22 shows a simulation for NIRSPEC observations in the 4.3  $\mu\text{m}$  region and its sensitivity to thermospheric temperatures. These authors concluded that variations of the order of 5 K could be achievable using these daytime signals, given the high sensitivity of NIRSPEC. ACS has a better spectral resolution but a lower sensitivity and should allow for similar determination during the ACS nominal nadir observing mode (1-10 s integration times).

The different viewpoint offers a challenge but a great potential for mutual validation and complementarity. The comparison of temperature maps built from a sequential mapping from ACS and from an instantaneous mapping from NIRSPEC should inform about the thermospheric temporal and spatial variability. Notice however that the JWST time periods for possible Mars observations are well defined and short, constrained by the JWST solar security angle, and this should dictate the preparation of the coordinated campaigns.

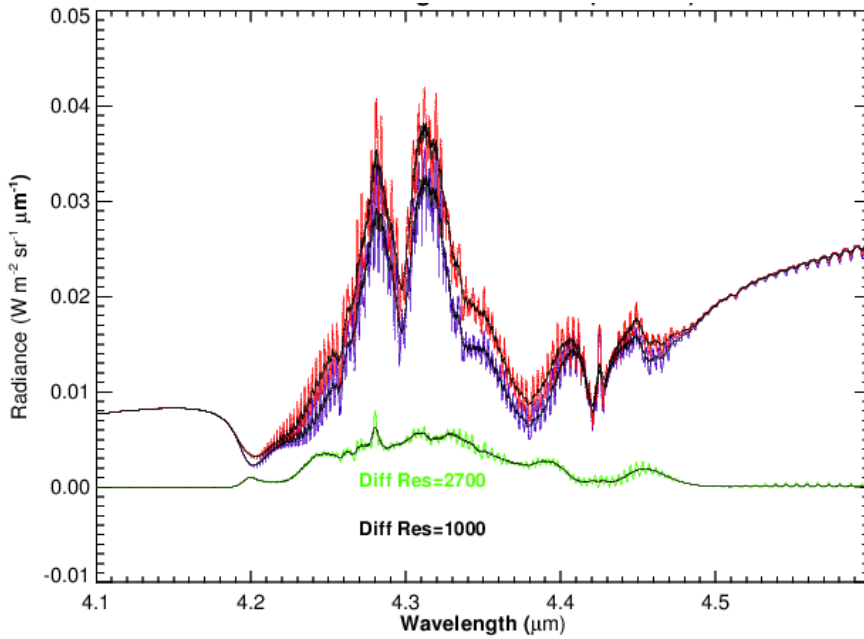


**Fig. 22** Simulation of nadir emission in the  $4.3 \mu\text{m}$  region as measured by the NIRSPEC instrument on board JWST and its sensitivity to changes in atmospheric temperatures. Purple lines: nominal emission for a SZA=60 degree; Red lines: with a 40 K warmer thermosphere. Figure reproduced from Villanueva et al., 2016 [134], with permission.

## 5 Summary and conclusions

This work reviews some interesting prospects of Exomars 2016 TGO to contribute to the science of the upper layers of the Martian atmosphere, both using the nominal operations and optional observing opportunities. We briefly discussed correlated or nearly coincident observations with on-going missions, specifically Maven, MRO and Mars Express, and future missions like JWST, which should be exploited as soon as TGO achieves its final regular orbit and such correlation campaigns can be effectively scheduled. Common science goals which should benefit from such cooperation include variability of the homopause, photochemical escape of water, wave coupling with the lower atmosphere, response of the upper atmosphere to solar inputs, climatology of thermospheric densities and temperatures, airglow detection and sources, tracers chemistry at the terminator and daily cycles, characterization of high altitude clouds, and validation of global climate models of Mars.

Table 2 presents a summary of these TGO capabilities. It includes the nominal operations (solar occultations, nadir mapping and aerobraking phase) and the possible limb sounding off-the-terminator strategies we recommend for specific upper atmosphere campaigns (see the four LSoft modes proposed in section 4.2 above). The table entries refer to targeted emissions from the UV to the IR, and are split in 3 sections according to the level of confidence in their detection. The first group, “Solid Predictions”, includes outputs of TGO observations expected to

**Table 2** Summary of TGO Capabilities for Upper Atmosphere Science

Confidence Level	Science Target	Topic <sup>♣</sup>	Nomad+ACS Channels	Observation Modes <sup>⊕</sup>
Solid Prediction	Lower-Upper atm couplings	IV,V	SO+MIR	Nominal S.Occ
	Diffusion & Escape processes	V	SO+MIR	Nominal S.Occ
	Improve UA <sup>†</sup> Climatologies (for CO <sub>2</sub> , CO, H <sub>2</sub> O, Temp., aerosols and clouds)	I - VII	SO+MIR+UVIS+NIR	Nominal S.Occ
	CO <sub>2</sub> Hot Bands & NLTE science	VI	SO+MIR	Nominal S.Occ
	Detect & Distinguish between dust & Ice aerosols. Study of bi-modal distributions	II,VII	SO+MIR +UVIS+NIR	Nominal S.Occ
	Latitudinal & Seasonal variability in Thermospheric Densities and Atmospheric Wave Propagation	II,III,IV,V		Aerobraking
	CO <sub>2</sub> VMR vs Total density	III,V,VI,VII		Aerobraking + Nominal S.Occ
	CO <sub>2</sub> daylight 4.3 um fluorescence	III,VI	TIRVIM	LSoffT 3, 4
Likely Detection	NO nightglow in NADIR	VI,VII	UVIS	Nominal Nadir mapping
	O <sub>3</sub> at the day-night transition	II,V,VI	UVIS	Nominal S.Occ
	Thermospheric temps from NADIR CO <sub>2</sub> fluorescence at 4.3 um	I,IV,VI,VII	TIRVIM	Nominal Nadir mapping
	NO Nightglow High Lats	VI,VII	UVIS	LSoffT 1, 2
	OH Meinel Bands in the polar night	VI	LNO+NIR	LSoffT 1, 2, 4
	Aurora in solar storms period	I,II,VI	UVIS	LSoffT 2
	O <sub>2</sub> 1.27 um Nightglow High Lats	II,VI,VII	NIR	LSoffT 2, 3
	UV dayglow and Thermospheric Temperatures from their limb profiles	I,VI	UVIS	LSoffT 2, 3, 4
	Very high altitude H <sub>2</sub> O ice clouds	III,V	NIR+UVIS	LSoffT 2, 3
Thermospheric Plumes	I,III,V,VI	LNO+NIR+UVIS(+TIRVIM)	LSoffT 1, 2, 3 (4)	
Difficult Target	First Detection of the O Green Line emission <sup>∇</sup>	VI	UVIS	LSoffT 1, 2
	Nightglow O <sub>2</sub> bands at high latitudes	VI,VII	UVIS	LSoffT 1, 2
	Visible Dayglow by CO <sub>2</sub> + and CO	III,VI	UVIS	LSoffT 1, 2
	CO <sub>2</sub> 2.7 um daylight fluorescence	IV,VI,VII	LNO	LSoffT 1-4
	NO 1.22 μm nightglow	VI,VII	NIR	LSoffT 2, 3, 4

<sup>⊕</sup> LSoffT stands for “limb sounding off-the-terminator” (see section 4.2 for details) :

LSoffT 1 = Limb pointing using NOMAD flip mirror

LSoffT 2 = Inertial limb scan

LSoffT 3 = Nadir boresight slew

LSoffT 4 = Fixed limb tracking

<sup>†</sup> UA stands for Upper Atmosphere

<sup>∇</sup> Best during active sun conditions

<sup>♣</sup> The roman numerals refer to the list of open topics in Section 2.

impact our understanding of the upper atmosphere which were already considered during the instruments’ design (except for the case of the CO<sub>2</sub> fluorescence at 4.3 μm). They are already incorporated into the primary targets of NOMAD and ACS (Vandaele et al., 2015 [132]; Korabev et al., 2017 [72]), and will be obtained during nominal operations modes.

The “Likely Detection” group includes emissions which are also expected to be observed but depend on factors like the final sensitivity on-orbit and the degree of binning of data that can be achieved (CO<sub>2</sub> IR dayglow and NO UV nightglow in

the TGO mapping modes), on the atmospheric intrinsic variability (NO, O<sub>3</sub>, O<sub>2</sub> and OH emissions), and also on the solar activity (auroral emissions), in addition to some degree of luck or serendipity (high altitude H<sub>2</sub>O clouds, thermospheric plumes). In addition to their intrinsic value, these targets would have very interesting applications, like the potential derivation of atmospheric temperatures off the terminator if the signals are strong. One obvious and additional condition for these data to be acquired is the actual implementation of the LSoft operations. We strongly recommend their incorporation into the science planning of TGO. The last group, labeled “Difficult Detections”, are weak emissions at or below the nominal detection limit and which will therefore require significant binning, but they do not require special operation modes other than those specified in the second “Likely” group.

A final consideration in this summary, is the benefit for upper atmosphere research of performing solar occultations at high beta angles. As we mentioned above, the increase in the mapping at low latitudes shown in Figure 5 would lead to a significant increase in interesting observations typically bounded to the equatorial zone, like thermal tides and CO<sub>2</sub> mesospheric clouds.

**Acknowledgements** The IAA/CSIC team has been supported by the European Union’s Horizon 2020 Programme (H2020-Compet-08-2014) under grant agreement UPWARDS-633127, by CSIC Proyecto Intramural 201450E022 and by the Plan Nacional del Espacio ESP2015-65064-C2-1-P (MINECO/FEDER). This research was partly supported by the SCOOP/BRAIN program of the Belgian Science Policy Office (BELSPO). We acknowledge the work of Sabrina Guilbon during her Master internship at LATMOS on the development of the technique to compare the slant profiles of SPICAM and the LMD GCM. M.R.P. thanks UKSA for support under grant ST/I003061/1 and ST/P001262/1. C.F.W. acknowledges funding support from the UK Space Agency. Work by A.K., D.J.M.C. and D.M.K. at the Jet Propulsion Laboratory, California Institute of Technology was performed under a contract with the National Aeronautics and Space Administration. OK, NI and AF thanks funding from Roscosmos for the ACS operation support and science funding from The Federal Agency of scientific organization (Planeta N<sup>o</sup> 0028-2014-0004).

## References

1. The atmosphere and climate of mars (cambridge planetary science) (2017). DOI 10.1017/97811139060172. URL [www.cambridge.org/9781107016187](http://www.cambridge.org/9781107016187)
2. Andrews, D.J., Barabash, S., Edberg, N.J.T., Gurnett, D.A., Hall, B.E.S., Holmström, M., Lester, M., Morgan, D.D., Opgenoorth, H.J., Ramstad, R., Sanchez-Cano, B., Way, M., Witasse, O.: Plasma observations during the mars atmospheric plume event of march-april 2012. *Journal of Geophysical Research: Space Physics* **121**(4), 3139–3154 (2016). DOI 10.1002/2015JA022023. URL <http://dx.doi.org/10.1002/2015JA022023>.
3. Barth, C., Stewart, A., Bougher, S., Hunten, D., Bauer, S., Nagy, A.: Aeronomy of the current martian atmosphere. In: C.S. H.H. Kieffer B.M. Jakosky, M. Matthews (eds.) *Mars*, pp. 1054–1089. University of Arizona Press, Tucson (1992)

4. Bertaux, J.L., Gondet, B., Lefèvre, F., Bibring, J.P., Montmessin, F.: First detection of O<sub>2</sub> 1.27  $\mu$ m nightglow emission at Mars with OMEGA/MEX and comparison with general circulation model predictions. *Journal of Geophysical Research (Planets)* **117**, E00J04 (2012). DOI 10.1029/2011JE003890
5. Bertaux, J.L., Leblanc, F., Perrier, S., Quemerais, E., Korablev, O., Dimarellis, E., Reberac, A., Forget, F., Simon, P.C., Stern, S.A., Sandel, B.: Nightglow in the upper atmosphere of mars and implications for atmospheric transport. *Science* **307**, 566–569 (2005). DOI 10.1126/science.1106957
6. Bertaux, J.L., Leblanc, F., Witasse, O., Quemerais, E., Lilensten, J., Stern, S.A., Sandel, B., Korablev, O.: Discovery of an aurora on Mars. *Nature* **435**, 790–794 (2005). DOI 10.1038/nature03603
7. Bougher, S., Jakosky, B., Halekas, J., Grebowsky, J., Luhmann, J., Mahaffy, P., Connerney, J., Eparvier, F., Ergun, R., Larson, D., McFadden, J., Mitchell, D., Schneider, N., Zurek, R., Mazelle, C., Andersson, L., Andrews, D., Baird, D., Baker, D.N., Bell, J.M., Benna, M., Brain, D., Chaffin, M., Chamberlin, P., Chaufray, J.Y., Clarke, J., Collinson, G., Combi, M., Crary, F., Cravens, T., Crismani, M., Curry, S., Curtis, D., Deighan, J., Delory, G., Dewey, R., DiBraccio, G., Dong, C., Dong, Y., Dunn, P., Elrod, M., England, S., Eriksson, A., Espley, J., Evans, S., Fang, X., Fillingim, M., Fortier, K., Fowler, C.M., Fox, J., Gröller, H., Guzewich, S., Hara, T., Harada, Y., Holsclaw, G., Jain, S.K., Jolitz, R., Leblanc, F., Lee, C.O., Lee, Y., Lefevre, F., Lillis, R., Livi, R., Lo, D., Ma, Y., Mayyasi, M., McClintock, W., McEnulty, T., Modolo, R., Montmessin, F., Morooka, M., Nagy, A., Olsen, K., Peterson, W., Rahmati, A., Ruhunusiri, S., Russell, C.T., Sakai, S., Sauvaud, J.A., Seki, K., Steckiewicz, M., Stevens, M., Stewart, A.I.F., Stiepen, A., Stone, S., Tennishev, V., Thiemann, E., Tolson, R., Toubanc, D., Vogt, M., Weber, T., Withers, P., Woods, T., Yelle, R.: Early maven deep dip campaign reveals thermosphere and ionosphere variability. *Science* **350**(6261) (2015). DOI 10.1126/science.aad0459. URL <http://science.sciencemag.org/content/350/6261/aad0459>
8. Bougher, S.W., Bell, J.M., Murphy, J.R., Lopez-Valverde, M.A., Withers, P.G.: Polar warming in the mars thermosphere: Seasonal variations owing to changing insolation and dust distributions. *Geophys. Res. Lett.* **33**, 2203–+ (2006). DOI 10.1029/2005GL024059
9. Bougher, S.W., Brain, A., Fox, J.L., Gonzalez-Galindo, F., Simon-Wedlund, C., Withers, P.G.: Chapter 14 - upper neutral atmosphere and ionosphere. In: B. Haberle, M. Smith, T. Clancy, F. Forget., R. Zurek (eds.) *The Atmosphere and Climate of Mars*, pp. 433–463. Cambridge University Press (2017). DOI 10.1017/9781139060172. URL [www.cambridge.org/9781107016187](http://www.cambridge.org/9781107016187)
10. Bougher, S.W., Cravens, T.E., Grebowsky, J., Luhmann, J.: The Aeronomy of Mars: Characterization by MAVEN of the Upper Atmosphere Reservoir That Regulates Volatile Escape. *Space Sci. Rev* (2014). DOI 10.1007/s11214-014-0053-7
11. Bougher, S.W., Pawlowski, D., Bell, J.M., Nelli, S., McDunn, T., Murphy, J.R., Chizek, M., Ridley, A.: Mars global ionosphere-thermosphere model: Solar cycle, seasonal, and diurnal variations of the mars upper atmosphere. *Journal of Geophysical Research: Planets* **120**(2), 311–342 (2015). DOI 10.1002/2014JE004715. URL <http://dx.doi.org/10.1002/2014JE004715>

12. Bougher, S.W., Roeten, K.J., Olsen, K., Mahaffy, P.R., Benna, M., Elrod, M., Jain, S.K., Schneider, N.M., Deighan, J., Thiemann, E., Eparvier, F.G., Stiepen, A., Jakosky, B.M.: The structure and variability of mars dayside thermosphere from maven ngims and iuvs measurements: Seasonal and solar activity trends in scale heights and temperatures. *Journal of Geophysical Research: Space Physics* **122**(1), 1296–1313 (2017). DOI 10.1002/2016JA023454. URL <http://dx.doi.org/10.1002/2016JA023454>
13. Bruinsma, S., Marty, J.C., Svedhem, H., Williams, A., Mueller-Wodarg, I.: Densities inferred from ESA’s Venus Express aerobraking campaign at 130 km altitude. In: EGU General Assembly Conference Abstracts, *EGU General Assembly Conference Abstracts*, vol. 17, p. 9841 (2015)
14. Chaffin, M.S., Chaufray, J.Y., Stewart, I., Montmessin, F., Schneider, N.M., Bertaux, J.L.: Unexpected variability of martian hydrogen escape. *Geophysical Research Letters* **41**(2), 314–320 (2014). DOI 10.1002/2013GL058578. URL <http://dx.doi.org/10.1002/2013GL058578>
15. Chaufray, J.Y., Gonzalez-Galindo, F., Forget, F., Lopez-Valverde, M., Leblanc, F., Modolo, R., Hess, S.: Variability of the hydrogen in the martian upper atmosphere as simulated by a 3d atmosphereexosphere coupling. *Icarus* **245**, 282 – 294 (2015). DOI <http://dx.doi.org/10.1016/j.icarus.2014.08.038>. URL <http://www.sciencedirect.com/science/article/pii/S0019103514004540>
16. Clancy, R.T., Sandor, B.J., García-Muñoz, A., Lefevre, F., Smith, M.D., Wolff, M.J., Montmessin, F., Murchie, S.L., Nair, H.: First detection of Mars atmospheric hydroxyl: CRISM Near-IR measurement versus LMD GCM simulation of OH Meinel band emission in the Mars polar winter atmosphere. *Icarus* **226**, 272–281 (2013). DOI 10.1016/j.icarus.2013.05.035
17. Clancy, R.T., Sandor, B.J., Wolff, M.J., Smith, M.D., Lefvre, F., Madeleine, J.B., Forget, F., Murchie, S.L., Seelos, F.P., Seelos, K.D., Nair, H.A., Toigo, A.D., Humm, D., Kass, D.M., Kleinbhl, A., Heavens, N.: Extensive mro crism observations of 1.27  $\mu$ m o<sub>2</sub> airglow in mars polar night and their comparison to mro mcs temperature profiles and lmd gcm simulations. *Journal of Geophysical Research: Planets* **117**(E11), n/a–n/a (2012). DOI 10.1029/2011JE004018. URL <http://dx.doi.org/10.1029/2011JE004018>
18. Clancy, R.T., Smith, M., Lefvère, F., Sandor, B., Wolff, M., McConnochie, T., Seelos, K., Nair, H., Toigo, A., Murchie, S.: CRISM Limb Observations of Coincident CO<sub>2</sub> Ice Clouds and O<sub>2</sub> Emission in the Mars Equatorial Mesosphere. In: AAS/Division for Planetary Sciences Meeting Abstracts, *AAS/Division for Planetary Sciences Meeting Abstracts*, vol. 47, p. 401.07 (2015)
19. Clancy, R.T., Smith, M.D., Lefvre, F., McConnochie, T.H., Sandor, B.J., Wolff, M.J., Lee, S.W., Murchie, S.L., Toigo, A.D., Nair, H., Navarro, T.: Vertical profiles of mars 1.27 $\mu$ m {O<sub>2</sub>} dayglow from {MRO} {CRISM} limb spectra: Seasonal/global behaviors, comparisons to {LMDGCM} simulations, and a global definition for mars water vapor profiles. *Icarus* **293**, 132 – 156 (2017). DOI <https://doi.org/10.1016/j.icarus.2017.04.011>. URL <http://www.sciencedirect.com/science/article/pii/S0019103516307217>
20. Clancy, R.T., Wolff, M.J., Lefvre, F., Cantor, B.A., Malin, M.C., Smith, M.D.: Daily global mapping of mars ozone column abundances with {MARCI} {UV} band imaging. *Icarus* **266**, 112 –

- 133 (2016). DOI <https://doi.org/10.1016/j.icarus.2015.11.016>. URL <http://www.sciencedirect.com/science/article/pii/S0019103515005266>
21. Clancy, R.T., Wolff, M.J., Whitney, B.A., Cantor, B.A., Smith, M.D., McConnochie, T.H.: Extension of atmospheric dust loading to high altitudes during the 2001 Mars dust storm: MGS TES limb observations. *Icarus* **207**, 98–109 (2010). DOI [10.1016/j.icarus.2009.10.011](https://doi.org/10.1016/j.icarus.2009.10.011)
22. Clarke, J.T., Bertaux, J.L., Chaufray, J.Y., Gladstone, G.R., Quemerais, E., Wilson, J.K., Bhattacharyya, D.: A rapid decrease of the hydrogen corona of mars. *Geophysical Research Letters* **41**(22), 8013–8020 (2014). DOI [10.1002/2014GL061803](https://doi.org/10.1002/2014GL061803). URL <http://dx.doi.org/10.1002/2014GL061803>. 2014GL061803
23. Clarke, J.T., Mayyasi, M., Bhattacharyya, D., Schneider, N.M., McClintock, W.E., Deighan, J.I., Stewart, A.I.F., Chaufray, J.Y., Chaffin, M.S., Jain, S.K., Stiepen, A., Crismani, M., Holsclaw, G.M., Montmessin, F., Jakosky, B.M.: Variability of d and h in the martian upper atmosphere observed with the maven iuvs echelle channel. *Journal of Geophysical Research: Space Physics* **122**(2), 2336–2344 (2017). DOI [10.1002/2016JA023479](https://doi.org/10.1002/2016JA023479). URL <http://dx.doi.org/10.1002/2016JA023479>. 2016JA023479
24. Coradini, A., Grassi, D., Capaccioni, F., Filacchione, G., Tosi, F., Ammannito, E., De Sanctis, M.C., Formisano, V., Wolkenberg, P., Rinaldi, G., Arnold, G., Barucci, M.A., Bellucci, G., Benkhoff, J., Bibring, J.P., Blanco, A., Bockelee-Morvan, D., Capria, M.T., Carlson, R., Carsenty, U., Cerroni, P., Colangeli, L., Combes, M., Combi, M., Crovisier, J., Drossart, P., Encrenaz, T., Erard, S., Federico, C., Fink, U., Fonti, S., Ip, W.H., Irwin, P.G.J., Jaumann, R., Kuehrt, E., Langevin, Y., Magni, G., McCord, T., Mennella, V., Mottola, S., Neukum, G., Orofino, V., Palumbo, P., Piccioni, G., Rauer, H., Schmitt, B., Tiphene, D., Taylor, F.W., Tozzi, G.P.: Martian atmosphere as observed by VIRTIS-M on Rosetta spacecraft. *Journal of Geophysical Research (Planets)* **115**, E04004 (2010). DOI [10.1029/2009JE003345](https://doi.org/10.1029/2009JE003345)
25. Cox, C., Sağlam, A., Gérard, J.C., Bertaux, J.L., González-Galindo, F., Leblanc, F., Reberac, A.: Distribution of the ultraviolet nitric oxide Martian night airglow: Observations from Mars Express and comparisons with a one-dimensional model. *Journal of Geophysical Research* **113**(E8), E08,012 (2008). DOI [10.1029/2007JE003037](https://doi.org/10.1029/2007JE003037). URL <http://doi.wiley.com/10.1029/2007JE003037>
26. de Kok, R., Irwin, P.G.J., Tsang, C.C.C., Piccioni, G., Drossart, P.: Scattering particles in nightside limb observations of Venus upper atmosphere by Venus Express VIRTIS. *Icarus* **211**, 51–57 (2011). DOI [10.1016/j.icarus.2010.08.023](https://doi.org/10.1016/j.icarus.2010.08.023)
27. Deighan, J., Stevens, M.H., Schneider, N.M., Jain, S.K., Lefèvre, F., Wolff, M., Montmessin, F., Stiepen, A., Evans, J.S., Chaffin, M.S., Crismani, M., Yelle, R.V., Lo, D.Y., Stewart, A.I.F., McClintock, W.E., Clarke, J.T., Holsclaw, G.M., Jakosky, B.M.: Characterization of High Altitude Clouds at the Martian Limb and Terminator Using MAVEN IUVS Observations. In: F. Forget, M. Millour (eds.) *The Mars Atmosphere: Modelling and observation*, p. 4101 (2017)
28. Dudhia, A.: The reference forward model (rfm). *Journal of Quantitative Spectroscopy and Radiative Transfer* **186**, 243 – 253 (2017). DOI [http://dx.doi.org/10.1016/j.jqsrt.2016.06.018](https://doi.org/10.1016/j.jqsrt.2016.06.018). URL

- <http://www.sciencedirect.com/science/article/pii/S0022407316301029>.  
Satellite Remote Sensing and Spectroscopy: Joint ACE-Odin Meeting, October 2015
29. Ehlmann, B.L., Anderson, F.S., Andrews-Hanna, J., Catling, D.C., Christensen, P.R., Cohen, B.A., Dressing, C.D., Edwards, C.S., Elkins-Tanton, L.T., Farley, K.A., Fassett, C.I., Fischer, W.W., Fraeman, A.A., Golombek, M.P., Hamilton, V.E., Hayes, A.G., Herd, C.D.K., Horgan, B., Hu, R., Jakosky, B.M., Johnson, J.R., Kasting, J.F., Kerber, L., Kinch, K.M., Kite, E.S., Knutson, H.A., Lunine, J.I., Mahaffy, P.R., Mangold, N., McCubbin, F.M., Mustard, J.F., Niles, P.B., Quantin-Nataf, C., Rice, M.S., Stack, K.M., Stevenson, D.J., Stewart, S.T., Toplis, M.J., Usui, T., Weiss, B.P., Werner, S.C., Wordsworth, R.D., Wray, J.J., Yingst, R.A., Yung, Y.L., Zahnle, K.J.: The sustainability of habitability on terrestrial planets: Insights, questions, and needed measurements from mars for understanding the evolution of earth-like worlds. *Journal of Geophysical Research: Planets* **121**(10), 1927–1961 (2016). DOI 10.1002/2016JE005134. URL <http://dx.doi.org/10.1002/2016JE005134>. 2016JE005134
  30. England, S.L., Liu, G., Withers, P., Yiğit, E., Lo, D., Jain, S., Schneider, N.M., Deighan, J., McClintock, W.E., Mahaffy, P.R., Elrod, M., Benna, M., Jakosky, B.M.: Simultaneous observations of atmospheric tides from combined in situ and remote observations at Mars from the MAVEN spacecraft. *Journal of Geophysical Research (Planets)* **121**, 594–607 (2016). DOI 10.1002/2016JE004997
  31. ESA: Esa robotic exploration of mars website (2016). URL <http://exploration.esa.int/mars>. Access date: 02 May 2016
  32. Evans, J.S., Stevens, M.H., Lumpe, J.D., Schneider, N.M., Stewart, A.I.F., Deighan, J., Jain, S.K., Chaffin, M.S., Crismani, M., Stiepen, A., McClintock, W.E., Holsclaw, G.M., Lefèvre, F., Lo, D.Y., Clarke, J.T., Eparvier, F.G., Thiemann, E.M.B., Chamberlin, P.C., Bougher, S.W., Bell, J.M., Jakosky, B.M.: Retrieval of CO<sub>2</sub> and N<sub>2</sub> in the Martian thermosphere using dayglow observations by IUVS on MAVEN. *Geophys. Res. Lett.* **42**, 9040–9049 (2015). DOI 10.1002/2015GL065489
  33. Fedorova, A., Bertaux, J.L., Montmessin, F., Korablev, O., Dzuban, I., Maltagliati, L., Clarke, J.: Water vapor in the middle atmosphere of Mars during the global dust storm in 2007. In: *EGU General Assembly Conference Abstracts*, *EGU General Assembly Conference Abstracts*, vol. 17, p. 8740 (2015)
  34. Fedorova, A., Lefvre, F., Guslyakova, S., Korablev, O., Bertaux, J.L., Montmessin, F., Reberac, A., Gondet, B.: The {O<sub>2</sub>} nightglow in the martian atmosphere by {SPICAM} onboard of mars-express. *Icarus* **219**(2), 596 – 608 (2012). DOI <https://doi.org/10.1016/j.icarus.2012.03.031>. URL <http://www.sciencedirect.com/science/article/pii/S0019103512001248>
  35. Fedorova, A.A., Korablev, O.I., Bertaux, J.L., Rodin, A.V., Montmessin, F., Belyaev, D.A., Reberac, A.: Solar infrared occultation observations by SPICAM experiment on Mars-Express: Simultaneous measurements of the vertical distributions of H<sub>2</sub>O, CO<sub>2</sub> and aerosol. *Icarus* **200**, 96–117 (2009). DOI 10.1016/j.icarus.2008.11.006
  36. Fedorova, A.A., Montmessin, F., Rodin, A.V., Korablev, O.I., Määttänen, A., Maltagliati, L., Bertaux, J.L.: Evidence for a bimodal size distribution for the suspended aerosol particles on Mars. *Icarus* **231**, 239–260 (2014).

- DOI 10.1016/j.icarus.2013.12.015
37. Forbes, J.M., Bridger, A.F.C., Bougher, S.W., Hagan, M.E., Hollingsworth, J.L., Keating, G.M., Murphy, J.: Nonmigrating tides in the thermosphere of mars. *J. Geophys. Res.* **107**, 23–1 (2002). DOI 10.1029/2001JE001582
  38. Forget, F., Millour, E., González-Galindo, F., Spiga, A., Lewis, S.R., Montabone, L., Read, P.L., López-Valverde, M.A., Gilli, G., Desjean, M.C., Huot, J.P., McD/Gcm Development Team: The new (version 4.2) mars climate database. *LPI Contributions* **1353**, 3098–+ (2007)
  39. Formisano, V., Maturilli, A., Giuranna, M., D’Aversa, E., López-Valverde, M.A.: Observations of non-lte emission at 4.5 microns with the planetary fourier spectrometer aboard the mars express mission. *Icarus* **182**, 51–67 (2006). DOI 10.1016/j.icarus.2005.12.022
  40. Fox, J.L., Dalgarno, A.: Ionization, luminosity, and heating of the upper atmosphere of Mars. *J. Geophys. Res.* **84**, 7315–7333 (1979). DOI 10.1029/JA084iA12p07315
  41. Fritts, D.C., Wang, L., Tolson, R.H.: Mean and gravity wave structures and variability in the mars upper atmosphere inferred from mars global surveyor and mars odyssey aerobraking densities. *Journal of Geophysical Research: Space Physics* **111**(A12), n/a–n/a (2006). DOI 10.1029/2006JA011897. URL <http://dx.doi.org/10.1029/2006JA011897>. A12304
  42. Gagné, M.E., Bertaux, J.L., González-Galindo, F., Melo, S.M.L., Montmessin, F., Strong, K.: New nitric oxide (NO) nightglow measurements with SPICAM/MEx as a tracer of Mars upper atmosphere circulation and comparison with LMD-MGCM model prediction: Evidence for asymmetric hemispheres. *Journal of Geophysical Research (Planets)* **118**, 2172–2179 (2013). DOI 10.1002/jgre.20165
  43. Gagné, M.È., Melo, S.M.L., Lefèvre, F., González-Galindo, F., Strong, K.: Modeled O<sub>2</sub> airglow distributions in the Martian atmosphere. *Journal of Geophysical Research (Planets)* **117**, E06005 (2012). DOI 10.1029/2011JE003901
  44. García Muñoz, A., Mills, F.P., Piccioni, G., Drossart, P.: The near-infrared nitric oxide nightglow in the upper atmosphere of venus. *Proceedings of the National Academy of Sciences* **106**(4), 985–988 (2009). DOI 10.1073/pnas.0808091106. URL <http://www.pnas.org/content/106/4/985.abstract>
  45. García Muñoz, A., Mills, F.P., Slanger, T.G., Piccioni, G., Drossart, P.: Visible and near-infrared nightglow of molecular oxygen in the atmosphere of venus. *Journal of Geophysical Research: Planets* **114**(E12), n/a–n/a (2009). DOI 10.1029/2009JE003447. URL <http://dx.doi.org/10.1029/2009JE003447>. E12002
  46. Gattinger, R.L., Lloyd, N.D., Bourassa, A.E., Degenstein, D.A., McDade, I.C., Llewellyn, E.J.: Observation of the 557.7nm to 297.2nm brightness ratio in the auroral spectrum with osiris on odin. *Canadian Journal of Physics* **87**(10), 1133–1137 (2009). DOI 10.1139/P09-102. URL <http://dx.doi.org/10.1139/P09-102>
  47. Gérard, J.C., Soret, L., Libert, L., Lundin, R., Stiepen, A., Radioti, A., Bertaux, J.L.: Concurrent observations of ultraviolet aurora and energetic electron precipitation with mars express. *Journal of Geophysical Research: Space Physics* **120**(8), 6749–6765 (2015). DOI 10.1002/2015JA021150. URL <http://dx.doi.org/10.1002/2015JA021150>. 2015JA021150

48. Gérard, J.C., Soret, L., Saglam, A., Piccioni, G., Drossart, P.: The distributions of the {OH} meinel and nightglow emissions in the venus mesosphere based on {VIRTIS} observations. *Advances in Space Research* **45**(10), 1268 – 1275 (2010). DOI <http://dx.doi.org/10.1016/j.asr.2010.01.022>. URL <http://www.sciencedirect.com/science/article/pii/S0273117710000578>
49. Gilli, G., López-Valverde, M.A., Drossart, P., Piccioni, G., Erard, S., Cardesín Moinelo, A.: Limb observations of CO<sub>2</sub> and CO non-LTE emissions in the venus atmosphere by VIRTIS/Venus Express. *J. Geophys. Res.* **114** (2009). DOI 10.1029/2008JE003112
50. Gilli, G., López-Valverde, M., Peralta, J., Bougher, S., Brecht, A., Drossart, P., Piccioni, G.: Carbon monoxide and temperature in the upper atmosphere of venus from VIRTIS/Venus Express non-LTE limb measurements. *Icarus* **248**(0), 478 – 498 (2015). DOI <http://dx.doi.org/10.1016/j.icarus.2014.10.047>. URL <http://www.sciencedirect.com/science/article/pii/S0019103514006137>
51. Giuranna, M., Wolkenberg, P., Grassi, D., Aronica, A., Aoki, S., Formisano, V., Scaccabarozzi, D., Saggin, B.: 12 Years of Atmospheric Monitoring by the Planetary Fourier Spectrometer onboard Mars Express. In: F. Forget, M. Millour (eds.) *The Mars Atmosphere: Modelling and observation*, p. 1203 (2017)
52. González-Galindo, F., Forget, F., López-Valverde, M.A., Angelats i Coll, M., Millour, E.: A ground-to-exosphere martian general circulation model: 1. seasonal, diurnal, and solar cycle variation of thermospheric temperatures. *Journal of Geophysical Research (Planets)* **114**(E13), 4001–+ (2009). DOI 10.1029/2008JE003246
53. González-Galindo, F., López-Valverde, M.A., Forget, F., García-Comas, M., Millour, E., Montabone, L.: Variability of the martian thermosphere during eight martian years as simulated by a ground-to-exosphere global circulation model. *Journal of Geophysical Research: Planets* **120**(11), 2020–2035 (2015). DOI 10.1002/2015JE004925. URL <http://dx.doi.org/10.1002/2015JE004925>
54. González-Galindo, F., Määttänen, A., Forget, F., Spiga, A.: The martian mesosphere as revealed by CO<sub>2</sub> cloud observations and General Circulation Modeling. *Icarus* **216**, 10–22 (2011). DOI 10.1016/j.icarus.2011.08.006
55. González-Galindo, F., Millour, E., López-Valverde, M.A., Forget, F., García-Comas, M., Chaufray, J.Y., Montabone, L.: Variability of the thermospheric temperatures given by the Imd-MGCM. In: *Mars Aeronomy Conference, Boulder CO* (2017)
56. Gray, C., Chanover, N., Slinger, T., Molaverdikhani, K.: The effect of solar flares, coronal mass ejections, and solar wind streams on venus 5577 oxygen green line. *Icarus* **233**, 342 – 347 (2014). DOI <http://dx.doi.org/10.1016/j.icarus.2014.01.029>. URL <http://www.sciencedirect.com/science/article/pii/S0019103514000608>
57. Gröller, H., Yelle, R.V., Koskinen, T.T., Montmessin, F., Lacombe, G., Schneider, N.M., Deighan, J., Stewart, A.I.F., Jain, S.K., Chaffin, M.S., Crismani, M.M.J., Stiepen, A., Lefèvre, F., McClintock, W.E., Clarke, J.T., Holsclaw, G.M., Mahaffy, P.R., Bougher, S.W., Jakosky, B.M.: Probing the Martian atmosphere with MAVEN/IUVS stellar occultations. *Geophys. Res. Lett.* **42**, 9064–9070 (2015). DOI 10.1002/2015GL065294

58. Guzewich, S.D., Talaat, E.R., Toigo, A.D., Waugh, D.W., McConnochie, T.H.: High-altitude dust layers on Mars: Observations with the Thermal Emission Spectrometer. *Journal of Geophysical Research (Planets)* **118**, 1177–1194 (2013). DOI 10.1002/jgre.20076
59. Heavens, N.G., Cantor, B., Hayne, P., Kass, D., Kleinbhl, A., McCleese, D., Piqueux, S., Schofield, J., Shirley, J.: Extreme detached dust layers near martian volcanoes: Evidence for dust transport by mesoscale circulations forced by high topography. Heavens, N. G., B.A. Cantor, P.O Hayne, D.M. Kass, A. Kleinbhl, D.J. McCleese, S. Piqueux, J.T. Schofield, and J.H. Shirley (2015). Extreme Detached Dust Layers near Martian Volcanoes: Evidence for Dust Transport by Mesoscale Circulations Forced by High Topography, *Geophys. Res. Lett.* **42**, 3730–3738, 10.1002/2015GL064004. **42**, 3730–3738 (2015). DOI 10.1002/2015GL064004
60. Heavens, N.G.e.a.: Seasonal and diurnal variability of detached dust layers in the tropical martian atmosphere. *J. Geophys. Res.* (2014). DOI 10.1002/2014JE004619
61. Imamura, T., Watanabe, A., Maejima, Y.: Convective generation and vertical propagation of fast gravity waves on mars: One- and two-dimensional modeling. *Icarus* **267**, 51 – 63 (2016). DOI <https://doi.org/10.1016/j.icarus.2015.12.005>. URL <http://www.sciencedirect.com/science/article/pii/S0019103515005552>
62. Jain, S.K., Stewart, A.I.F., Schneider, N.M., Deighan, J., Stiepen, A., Evans, J.S., Stevens, M.H., Chaffin, M.S., Crismani, M., McClintock, W.E., Clarke, J.T., Holsclaw, G.M., Lo, D.Y., Lefèvre, F., Montmessin, F., Thiemann, E.M.B., Eparvier, F., Jakosky, B.M.: The structure and variability of Mars upper atmosphere as seen in MAVEN/IUVS dayglow observations. *Geophys. Res. Lett.* **42**, 9023–9030 (2015). DOI 10.1002/2015GL065419
63. Jakosky, B., Lin, R., Grebowsky, J., Luhmann, J., Mitchell, D., Beutelschies, G., Priser, T., Acuna, M., Andersson, L., Baird, D., Baker, D., Bartlett, R., Benna, M., Bougher, S., Brain, D., Carson, D., Cauffman, S., Chamberlin, P., Chaufray, J.Y., Cheatom, O., Clarke, J., Connerney, J., Cravens, T., Curtis, D., Delory, G., Demcak, S., DeWolfe, A., Eparvier, F., Ergun, R., Eriksson, A., Espley, J., Fang, X., Folta, D., Fox, J., Gomez-Rosa, C., Habenicht, S., Halekas, J., Holsclaw, G., Houghton, M., Howard, R., Jarosz, M., Jedrich, N., Johnson, M., Kasprzak, W., Kelley, M., King, T., Lankton, M., Larson, D., Leblanc, F., Lefevre, F., Lillis, R., Mahaffy, P., Mazelle, C., McClintock, W., McFadden, J., Mitchell, D., Montmessin, F., Morrissey, J., Peterson, W., Pospel, W., Sauvaud, J.A., Schneider, N., Sidney, W., Sparacino, S., Stewart, A., Tolson, R., Toubanc, D., Waters, C., Woods, T., Yelle, R., Zurek, R.: The mars atmosphere and volatile evolution (maven) mission. *Space Science Reviews* pp. 1–46 (2015). DOI 10.1007/s11214-015-0139-x. URL <http://dx.doi.org/10.1007/s11214-015-0139-x>
64. Jakosky, B.M., Slipski, M., Benna, M., Mahaffy, P., Elrod, M., Yelle, R., Stone, S., Alsaeed, N.: Mars’ atmospheric history derived from upper-atmosphere measurements of 38ar/36ar. *Science* **355**(6332), 1408–1410 (2017). DOI 10.1126/science.aai7721. URL <http://science.sciencemag.org/content/355/6332/1408>
65. Justh, H.L., Justus, C.G., Ramey, H.S.: Mars-Gram 2010: Improving the precision of Mars-Gram. In: F. Forget, E. Millour (eds.) *Mars Atmosphere:*

- Modelling and observation, pp. 265–267 (2011)
66. Kass, D.M., Kleinbhl, A., McCleese, D.J., Schofield, J.T., Smith, M.D.: Interannual similarity in the martian atmosphere during the dust storm season. *Geophysical Research Letters* **43**(12), 6111–6118 (2016). DOI 10.1002/2016GL068978. URL <http://dx.doi.org/10.1002/2016GL068978>.
  67. Keating, G.M., Bougher, S.W., Zurek, R.W., Tolson, R.H., Cancro, G.J., Noll, S.N., Parker, J.S., Schellenberg, T.J., Shane, R.W., Wilkerson, B.L., Murphy, J.R., Hollingsworth, J.L., Haberle, R.M., Joshi, M., Pearl, J.C., Conrath, B.J., Smith, M.D., Clancy, R.T., Blanchard, R.C., Wilmoth, R.G., Rault, D.F., Martin, T.Z., Lyons, D.T., Esposito, P.B., Johnston, M.D., Whetzel, C.W., Justus, C.G., Babicke, J.M.: The structure of the upper atmosphere of mars: In situ accelerometer measurements from mars global surveyor. *Science* **279**, 1672–+ (1998). DOI 10.1126/science.279.5357.1672
  68. Kleinböhl, A., John Wilson, R., Kass, D., Schofield, J.T., McCleese, D.J.: The semidiurnal tide in the middle atmosphere of mars. *Geophysical Research Letters* **40**(10), 1952–1959 (2013). DOI 10.1002/grl.50497. URL <http://dx.doi.org/10.1002/grl.50497>
  69. Kleinböhl, A., Schofield, J.T., Abdou, W.A., Irwin, P.G., de Kok, R.J.: A single-scattering approximation for infrared radiative transfer in limb geometry in the martian atmosphere. *Journal of Quantitative Spectroscopy and Radiative Transfer* **112**(10), 1568 – 1580 (2011). DOI <http://dx.doi.org/10.1016/j.jqsrt.2011.03.006>. URL <http://www.sciencedirect.com/science/article/pii/S0022407311001166>
  70. Kleinböhl, A., Schofield, J.T., Kass, D.M., Abdou, W.a., Backus, C.R., Sen, B., Shirley, J.H., Lawson, W.G., Richardson, M.I., Taylor, F.W., Teanby, N.a., McCleese, D.J.: Mars Climate Sounder limb profile retrieval of atmospheric temperature, pressure, and dust and water ice opacity. *Journal of Geophysical Research* **114**(E10), E10,006 (2009). DOI 10.1029/2009JE003358. URL <http://doi.wiley.com/10.1029/2009JE003358>
  71. Kleinbhl, A., Friedson, A.J., Schofield, J.T.: Two-dimensional radiative transfer for the retrieval of limb emission measurements in the martian atmosphere. *J. Quant. Spectr. Rad. Trans.* **187**, 511–522. (2017)
  72. Korablev, O., Montmessin, F., Trokhimovskiy, A., A.-A, Fedorova, Shakun, A.V., Grigoriev, A.V., Moshkin, B., Ignatiev, N., Forget, F., Lefvre, F., Anufreychik, K., Kozlova, T., Semena, N., Ivanov, Y., Kungurov, A., Kalinikov, Y.K., Titov, A.Y., Stepanov, A.V., Zharkov, A., Semenov, A., Patsaev, D., Martynovich, F., Sidorov, A., Viktorov, A., Timonin, D., Sazonov, O., Shashkin, V., Santos-Skripko, A., Maslov, I., Dzuban, I., Stupin, I., Merzlyakov, D., Makarov, V., Nikolskiy, Y., Altieri, F., Arnold, G., Belyaev, D.A., Betsis, D.S., Bertaux, J.L., Duxbury, N., Encrenaz, T., Gerard, J.C., Guerlet, S., Grassi, D., Fouchet, T., Hartogh, P., Kasaba, Y., Khatuntsev, I., Krasnopolsky, V.A., Kuzmin, R.O., Lellouch, E., Lopez-Valverde, M.A., Luginin, M., Mtnen, A., Marcq, E., Torres, J.M., Medvedev, A., Millour, E., Shematovich, V.I., Olsen, K., Patel, M., Quantin-Nataf, C., Rodin, A.V., Thomas, I., Thomas, N., Vazquez, L., Vincendon, M., Wilquet, V., Wilson, C., Zasova, L.V., Zelenyi, L.M., Zorzano, M.P.: The atmospheric chemistry suite (acs) of three spectrometers for the exomars 2016 trace gas orbiter. *Space Sci. Rev* (2017)

73. Korablev, O.I., Montmessin, F., Fedorova, A.A., Ignatiev, N.I., Shakun, A.V., Trokhimovskiy, A.V., Grigoriev, A.V., Anufreichik, K.A., Kozlova, T.O.: Acs experiment for atmospheric studies on “exomars-2016” orbiter. *Solar System Research* **49**(7), 529–537 (2015). DOI 10.1134/S003809461507014X. URL <http://dx.doi.org/10.1134/S003809461507014X>
74. Leblanc, F., Chaufray, J.Y., Lilensten, J., Witasse, O., Bertaux, J.L.: Martian dayglow as seen by the SPICAM UV spectrograph on Mars Express. *Journal of Geophysical Research* **111**(E9), E09S11 (2006). DOI 10.1029/2005JE002664. URL <http://doi.wiley.com/10.1029/2005JE002664>
75. Lebonnois, S., Quémerais, E., Montmessin, F., Lefèvre, F., Perrier, S., Bertaux, J.L., Forget, F.: Vertical distribution of ozone on mars as measured by spicam/mars express using stellar occultations. *Journal of Geophysical Research (Planets)* **111**, 9+ (2006). DOI 10.1029/2005JE002643
76. Lee, C., Lawson, W.G., Richardson, M.I., Heavens, N.G., Kleinböhl, a., Banfield, D., McCleese, D.J., Zurek, R., Kass, D., Schofield, J.T., Leovy, C.B., Taylor, F.W., Toigo, a.D.: Thermal tides in the Martian middle atmosphere as seen by the Mars Climate Sounder. *Journal of Geophysical Research* **114**(E3), E03,005 (2009). DOI 10.1029/2008JE003285. URL <http://doi.wiley.com/10.1029/2008JE003285>
77. Lilensten, J., Bernard, D., Barthlmy, M., Gronoff, G., Wedlund, C.S., Opitz, A.: Prediction of blue, red and green aurorae at mars. *Planetary and Space Science* **115**, 48 – 56 (2015). DOI <http://dx.doi.org/10.1016/j.pss.2015.04.015>. URL <http://www.sciencedirect.com/science/article/pii/S0032063315001300>. Solar wind interaction with the terrestrial planets
78. Limaye, S.S., Lebonnois, S., Mahieux, A., Ptzold, M., Bougher, S., Bruinsma, S., Chamberlain, S., Clancy, R.T., Grard, J.C., Gilli, G., Grassi, D., Haus, R., Herrmann, M., Imamura, T., Kohler, E., Krause, P., Migliorini, A., Montmessin, F., Pere, C., Persson, M., Piccialli, A., Rengel, M., Rodin, A., Sandor, B., Sornig, M., Svedhem, H., Tellmann, S., Tanga, P., Vandaele, A.C., Widemann, T., Wilson, C.F., Miller-Wodarg, I., Zasova, L.: The thermal structure of the venus atmosphere: Intercomparison of venus express and ground based observations of vertical temperature and density profiles? *Icarus* **294**, 124 – 155 (2017). DOI <https://doi.org/10.1016/j.icarus.2017.04.020>. URL <http://www.sciencedirect.com/science/article/pii/S0019103516307138>
79. López-Puertas, M., Funke, B., Gil-López, S., von Clarmann, T., Stiller, G.P., Höpfner, M., Kellmann, S., Mengistu Tsidu, G., Fischer, H., Jackman, C.H.: HNO<sub>3</sub>, N<sub>2</sub>O<sub>5</sub> and ClONO<sub>2</sub> enhancements after the October–November 2003 solar proton events. *J. Geophys. Res.* **110**(A9), A09S44 (2005). DOI 10.1029/2005JA011051
80. López-Puertas, M., Taylor, F.W.: Non-LTE radiative transfer in the Atmosphere. World Scientific Pub., Singapore (2001)
81. Lopez-Valverde, M.A., García-Comas, M., Funke, B., Jimenez-Monferrer, S., Lopez-Puertas, M.: A non-LTE retrieval scheme for sounding the upper atmosphere of Mars in the infrared. In: EGU General Assembly Conference Abstracts, *EGU General Assembly Conference Abstracts*, vol. 18, p. 17281 (2016)

82. Lopez-Valverde, M.A., Lopez-Puertas, M.: A non-local thermodynamic equilibrium radiative transfer model for infrared emission in the atmosphere of Mars. 2: Daytime populations of vibrational levels. *J. Geophys. Res.* **99**, 13,117–13,132 (1994). DOI 10.1029/94JE01091
83. Lopez-Valverde, M.A., Lopez-Puertas, M.: A non-local thermodynamic equilibrium radiative transfer model for infrared emissions in the atmosphere of Mars. 1: Theoretical basis and nighttime populations of vibrational levels. *J. Geophys. Res.* **99**, 13,093–13,115 (1994). DOI 10.1029/94JE00635
84. López-Valverde, M.A., López-Puertas, M., Funke, B., Gilli, G., García-Comas, M., Drossart, P., Piccioni, G., Formisano, V., Valverde: Modelling the Atmospheric Limb Emission of CO<sub>2</sub> at 4.3  $\mu\text{m}$  in the Terrestrial Planets. *Planet. Space Sci.* **59**, 988–998 (2011). DOI DOI: 10.1016/j.pss.2010.02.001. URL <http://www.sciencedirect.com/science/article/B6V6T-4YDC3P0-1/2/e4a1f2a46f24d2ac2af373a16906c334>
85. Lopez-Valverde, M.A., Montabone, L., Sornig, M., Sonnabend, G.: On the retrieval of mesospheric winds on mars and venus from ground-based observations at 10 m. *The Astrophysical Journal* **816**(2), 103 (2016). URL <http://stacks.iop.org/0004-637X/816/i=2/a=103>
86. Määttänen, A., Listowski, C., Montmessin, F., Maltagliati, L., Reberac, A., Joly, L., Bertaux, J.L.: A complete climatology of the aerosol vertical distribution on Mars from MEx/SPICAM UV solar occultations. *Icarus* **223**, 892–941 (2013). DOI 10.1016/j.icarus.2012.12.001
87. Madeleine, J.B., Head, J.W., Forget, F., Navarro, T., Millour, E., Spiga, A., Colatis, A., Mttnen, A., Montmessin, F., Dickson, J.L.: Recent ice ages on mars: The role of radiatively active clouds and cloud microphysics. *Geophysical Research Letters* **41**(14), 4873–4879 (2014). DOI 10.1002/2014GL059861. URL <http://dx.doi.org/10.1002/2014GL059861>
88. Mahaffy, P.R., Benna, M., Elrod, M., Yelle, R.V., Bougher, S.W., Stone, S.W., Jakosky, B.M.: Structure and composition of the neutral upper atmosphere of Mars from the MAVEN NGIMS investigation. *Geophys. Res. Lett.* **42**, 8951–8957 (2015). DOI 10.1002/2015GL065329
89. Mahieux, A., Bellucci, G., Aoki, S., Wolkenberg, P., Iwabuchi, H., Kasaba, Y., Nakagawa, H., Giuranna, M., Vandaele, A.C.: Retrieval of Gas and Aerosols Vertical Profiles by Means of Limb Observations Considering Multiple Scattering of the PFS/MEx and NOMAD/ExoMars Instruments. In: F. Forget, M. Millour (eds.) *The Mars Atmosphere: Modelling and observation*, p. 4409 (2017)
90. Mahieux, A., Vandaele, A., Bougher, S., Drummond, R., Robert, S., Wilquet, V., Chamberlain, S., Piccialli, A., Montmessin, F., Tellmann, S., Ptzold, M., Husler, B., Bertaux, J.: Update of the venus density and temperature profiles at high altitude measured by soir on board venus express. *Planetary and Space Science* pp. – (2015). DOI <http://dx.doi.org/10.1016/j.pss.2015.02.002>. URL <http://www.sciencedirect.com/science/article/pii/S0032063315000343>
91. Mahieux, A., Vandaele, A., Robert, S., Wilquet, V., Drummond, R., Valverde, M.L., Puertas, M.L., Funke, B., Bertaux, J.: Rotational temperatures of venus upper atmosphere as measured by {SOIR} on board venus express. *Planet. Space Sci.* **113114**, 347 – 358 (2015). DOI 10.1016/j.pss.2014.12.020. URL <http://www.sciencedirect.com/science/article/pii/S0032063314004218>

92. Mahieux, A., Vandaele, A.C., Neefs, E., Robert, S., Wilquet, V., Drummond, R., Federova, A., Bertaux, J.L.: Densities and temperatures in the Venus mesosphere and lower thermosphere retrieved from SOIR on board Venus Express: Retrieval technique. *Journal of Geophysical Research (Planets)* **115**(E14), 12,014–+ (2010). DOI 10.1029/2010JE003589
93. Malin, M.C., Calvin, W.M., Cantor, B.A., Clancy, R.T., Haberle, R.M., James, P.B., Thomas, P.C., Wolff, M.J., III, J.F.B., Lee, S.W.: Climate, weather, and north polar observations from the mars reconnaissance orbiter mars color imager. *Icarus* **194**(2), 501 – 512 (2008). DOI <https://doi.org/10.1016/j.icarus.2007.10.016>. URL <http://www.sciencedirect.com/science/article/pii/S0019103507005519>
94. Maltagliati, L., Montmessin, F., Korablev, O., Fedorova, A., Forget, F., Mttnen, A., Lefvre, F., Bertaux, J.L.: Annual survey of water vapor vertical distribution and water? aerosol coupling in the martian atmosphere observed by spicam/mex solar occultations. *Icarus* **223**(2), 942 – 962 (2013). DOI <https://doi.org/10.1016/j.icarus.2012.12.012>. URL <http://www.sciencedirect.com/science/article/pii/S0019103512005064>
95. McCleese, D.J., Schofield, J.T., Taylor, F.W., Calcutt, S.B., Foote, M.C., Kass, D.M., Leovy, C.B., Paige, D.A., Read, P.L., Zurek, R.W.: Mars climate sounder: An investigation of thermal and water vapor structure, dust and condensate distributions in the atmosphere, and energy balance of the polar regions. *Journal of Geophysical Research: Planets* **112**(E5), n/a–n/a (2007). DOI 10.1029/2006JE002790. URL <http://dx.doi.org/10.1029/2006JE002790>. E05S06
96. Medvedev, A.S., Gonzalez-Galindo, F., Yi?it, E., Feofilov, A.G., Forget, F., Hartogh, P.: Cooling of the martian thermosphere by co2 radiation and gravity waves: An intercomparison study with two general circulation models. *Journal of Geophysical Research: Planets* **120**(5), 913–927 (2015). DOI 10.1002/2015JE004802. URL <http://dx.doi.org/10.1002/2015JE004802>. 2015JE004802
97. Migliorini, A., Piccioni, G., Grard, J., Soret, L., Slanger, T., Politi, R., Snels, M., Drossart, P., Nuccilli, F.: The characteristics of the {O2} herzberg {II} and chamberlain bands observed with virtis/venus express. *Icarus* **223**(1), 609 – 614 (2013). DOI <http://dx.doi.org/10.1016/j.icarus.2012.11.017>. URL <http://www.sciencedirect.com/science/article/pii/S001910351200471X>
98. Millour, E., Forget, F., Spiga, A., Navarro, T., Madeleine, J.B., Montabone, L., Pottier, A., Lefevre, F., Montmessin, F., Chaufray, J.Y., Lopez-Valverde, M.A., Gonzalez-Galindo, F., Lewis, S.R., Read, P.L., Huot, J.P., Desjean, M.C., MCD/GCM development Team: The Mars Climate Database (MCD version 5.2). *European Planetary Science Congress 2015, held 27 September - 2 October, 2015 in Nantes, France* **10**, EPSC2015-438 (2015)
99. Montmessin, F., Lefèvre, F.: Transport-driven formation of a polar ozone layer on Mars. *Nature Geoscience* **6**, 930–933 (2013). DOI 10.1038/ngeo1957
100. Montmessin, F., Quèmerais, E., Bertaux, J.L., Korablev, O., Rannou, P., Lebonnois, S.: Stellar occultations at uv wavelengths by the spicam instrument: Retrieval and analysis of martian haze profiles. *Journal of Geophysical Research: Planets* **111**(E9) (2006). DOI 10.1029/2005JE002662. URL <http://dx.doi.org/10.1029/2005JE002662>

101. Moudden, Y., Forbes, J.M.: A new interpretation of mars aerobraking variability: Planetary wave-tide interactions. *Journal of Geophysical Research: Planets* **115**(E9), n/a–n/a (2010). DOI 10.1029/2009JE003542. URL <http://dx.doi.org/10.1029/2009JE003542>. E09005
102. Muller-Wodarg, I.C.F., Bruinsma, S., Marty, J.C., Svedhem, H.: In situ observations of waves in venus's polar lower thermosphere with venus express aerobraking. *Nat Phys* **12**(8), 767–771 (2016). URL <http://dx.doi.org/10.1038/nphys3733>. Letter
103. Murchie, S., Arvidson, R., Bedini, P., Beisser, K., Bibring, J.P., Bishop, J., Boldt, J., Cavender, P., Choo, T., Clancy, R.T., Darlington, E.H., Des Marais, D., Espiritu, R., Fort, D., Green, R., Guinness, E., Hayes, J., Hash, C., Hefferman, K., Hemmler, J., Heyler, G., Humm, D., Hutcheson, J., Izenberg, N., Lee, R., Lees, J., Lohr, D., Malaret, E., Martin, T., McGovern, J.A., McGuire, P., Morris, R., Mustard, J., Pelkey, S., Rhodes, E., Robinson, M., Roush, T., Schaefer, E., Seagrave, G., Seelos, F., Silverglate, P., Slavney, S., Smith, M., Shyong, W.J., Strohbehn, K., Taylor, H., Thompson, P., Tossman, B., Wirzburger, M., Wolff, M.: Compact reconnaissance imaging spectrometer for mars (crism) on mars reconnaissance orbiter (mro). *Journal of Geophysical Research: Planets* **112**(E5), n/a–n/a (2007). DOI 10.1029/2006JE002682. URL <http://dx.doi.org/10.1029/2006JE002682>. E05S03
104. Navarro, T., Madeleine, J.B., Forget, F., Spiga, A., Millour, E., Montmessin, F., Mttnen, A.: Global climate modeling of the martian water cycle with improved microphysics and radiatively active water ice clouds. *Journal of Geophysical Research: Planets* **119**(7), 1479–1495 (2014). DOI 10.1002/2013JE004550. URL <http://dx.doi.org/10.1002/2013JE004550>
105. Neefs, E., Vandaele, A.C., Drummond, R., Thomas, I.R., Berkenbosch, S., Clairquin, R., Delanoye, S., Ristic, B., Maes, J., Bonnewijn, S., Pieck, G., Equeter, E., Depiesse, C., Daerden, F., Ransbeeck, E.V., Nevejans, D., Rodriguez-Gómez, J., López-Moreno, J.J., Sanz, R., Morales, R., Candini, G.P., Pastor-Morales, M.C., del Moral, B.A., Jeronimo-Zafra, J.M., Gómez-López, J.M., Alonso-Rodrigo, G., Pérez-Grande, I., Cubas, J., Gomez-Sanjuan, A.M., Navarro-Medina, F., Thibert, T., Patel, M.R., Bellucci, G., Vos, L.D., Lesschaeve, S., Vooren, N.V., Moelans, W., Aballea, L., Glorieux, S., Baeke, A., Kendall, D., Neef, J.D., Soenen, A., Puech, P.Y., Ward, J., Jamoye, J.F., Diez, D., Vicario-Arroyo, A., Jankowski, M.: Nomad spectrometer on the exomars trace gas orbiter mission: part 1&#x2014;design, manufacturing and testing of the infrared channels. *Appl. Opt.* **54**(28), 8494–8520 (2015). DOI 10.1364/AO.54.008494. URL <http://ao.osa.org/abstract.cfm?URI=ao-54-28-8494>
106. Patel, M.R., Antoine, P., Mason, J., Leese, M., Hathi, B., Stevens, A.H., Dawson, D., Gow, J., Ringrose, T., Holmes, J., Lewis, S.R., Beghuin, D., van Donink, P., Ligot, R., Dewandel, J.L., Hu, D., Bates, D., Cole, R., Drummond, R., Thomas, I.R., Depiesse, C., Neefs, E., Equeter, E., Ristic, B., Berkenbosch, S., Bolsée, D., Willame, Y., Vandaele, A.C., Lesschaeve, S., Vos, L.D., Vooren, N.V., Thibert, T., Mazy, E., Rodriguez-Gomez, J., Morales, R., Candini, G.P., Pastor-Morales, M.C., Sanz, R., del Moral, B.A., Jeronimo-Zafra, J.M., Gómez-López, J.M., Alonso-Rodrigo, G., Pérez-Grande, I., Cubas, J., Gomez-Sanjuan, A.M., Navarro-Medina, F., Ben-Moussa, A., Giordanengo, B., Gissot, S., Bellucci, G., Lopez-Moreno, J.J.:

- Nomad spectrometer on the exomars trace gas orbiter mission: part 2—design, manufacturing, and testing of the ultraviolet and visible channel. *Appl. Opt.* **56**(10), 2771–2782 (2017). DOI 10.1364/AO.56.002771. URL <http://ao.osa.org/abstract.cfm?URI=ao-56-10-2771>
107. Peralta, J., López-Valverde, M.A., Gilli, G., Piccialli, A.: Dayside temperatures in the Venus upper atmosphere from Venus Express/VIRTIS nadir measurements at 4.3  $\mu\text{m}$ . *A&A* **585**, A53 (2016). DOI 10.1051/0004-6361/201527191
108. Piccialli, A., López-Valverde, M.A., Määttäänen, A., González-Galindo, F., Audouard, J., Altieri, F., Forget, F., Drossart, P., Gondet, B., Bibring, J.P.: Co<sub>2</sub> non-lte limb emissions in mars' atmosphere as observed by omega/mars express. *Journal of Geophysical Research: Planets* **121**(6), 1066–1086 (2016). DOI 10.1002/2015JE004981. URL <http://dx.doi.org/10.1002/2015JE004981>
109. Piccialli, A., Montmessin, F., Belyaev, D., Mahieux, A., Fedorova, A., Marcq, E., Bertaux, J.L., Tellmann, S., Vandaele, A., Korablev, O.: Thermal structure of venus nightside upper atmosphere measured by stellar occultations with spicav/venus express. *Planetary and Space Science* **113?114**, 321 – 335 (2015). DOI <https://doi.org/10.1016/j.pss.2014.12.009>. URL <http://www.sciencedirect.com/science/article/pii/S0032063314004012>. SI:Exploration of Venus
110. Piccioni, G., Drossart, P., Zasova, L., Migliorini, A., Gérard, J.-C., Mills, F. P., Shakun, A., García Muñoz, A., Ignatiev, N., Grassi, D., Cottini, V., Taylor, F. W., Erard, S., the VIRTIS-Venus Express Technical Team: First detection of hydroxyl in the atmosphere of venus. *A&A* **483**(3), L29–L33 (2008). DOI 10.1051/0004-6361:200809761. URL <http://dx.doi.org/10.1051/0004-6361:200809761>
111. Robert, S., Camy-Peyret, C., Daerden, F., Mazire, M.D., Wachter, E.D., Neary, L., Vandebussche, S., Vandaele, A.: Two test-cases for synergistic detections in the martian atmosphere: Carbon monoxide and methane. *Journal of Quantitative Spectroscopy and Radiative Transfer* **189**, 86 – 104 (2017). DOI <https://doi.org/10.1016/j.jqsrt.2016.11.003>. URL <http://www.sciencedirect.com/science/article/pii/S0022407316300632>
112. Robert, S., Vandaele, A., Thomas, I., Willame, Y., Daerden, F., Delanoye, S., Depiesse, C., Drummond, R., Neefs, E., Neary, L., Ristic, B., Mason, J., Lopez-Moreno, J.J., Rodriguez-Gomez, J., Patel, M., Bellucci, G., the NOMAD team: Expected performances of the nomad/exomars instrument. *Planetary and Space Science* **124**, 94 – 104 (2016). DOI <http://dx.doi.org/10.1016/j.pss.2016.03.003>. URL <http://www.sciencedirect.com/science/article/pii/S0032063315301203>
113. R.W., Z., S.E., S.: An overview of the mars reconnaissance orbiter (mro) science mission. *J. Geophys. Res.* (2007). DOI 10.1029/2006JE002701
114. Sanchez-Lavega, A., Munoz, A.G., Garcia-Melendo, E., Perez-Hoyos, S., Gomez-Forrellad, J.M., Pellier, C., Delcroix, M., Lopez-Valverde, M.A., Gonzalez-Galindo, F., Jaeschke, W., Parker, D., Phillips, J., Peach, D.: An extremely high-altitude plume seen at mars/' morning terminator. *Nature* **advance online publication** (2015). URL <http://dx.doi.org/10.1038/nature14162>. Letter

115. Schneider, N.M., Deighan, J.I., Jain, S.K., Stiepen, A., Stewart, A.I.F., Larson, D., Mitchell, D.L., Mazelle, C., Lee, C.O., Lillis, R.J., Evans, J.S., Brain, D., Stevens, M.H., McClintock, W.E., Chaffin, M.S., Crismani, M., Holsclaw, G.M., Lefevre, F., Lo, D.Y., Clarke, J.T., Montmessin, F., Jakosky, B.M.: Discovery of diffuse aurora on mars. *Science* **350**(6261) (2015). DOI 10.1126/science.aad0313. URL <http://science.sciencemag.org/content/350/6261/aad0313>
116. Slanger, T.G., Cosby, P.C., Huestis, D.L., Bida, T.A.: Discovery of the atomic oxygen green line in the venus night airglow. *Science* **291**(5503), 463–465 (2001). DOI 10.1126/science.291.5503.463. URL <http://science.sciencemag.org/content/291/5503/463>
117. Smith, M.D., Wolff, M.J., Clancy, R.T., Murchie, S.L.: Compact reconnaissance imaging spectrometer observations of water vapor and carbon monoxide. *Journal of Geophysical Research: Planets* **114**(E2), n/a–n/a (2009). DOI 10.1029/2008JE003288. URL <http://dx.doi.org/10.1029/2008JE003288>. E00D03
118. Song, R., Kaufmann, M., Ungermann, J., Ern, M., Liu, G., Riese, M.: Tomographic reconstruction of atmospheric gravity wave parameters from airglow observations. *Atmospheric Measurement Techniques Discussions* **2017**, 1–18 (2017). DOI 10.5194/amt-2017-118. URL <http://www.atmos-meas-tech-discuss.net/amt-2017-118/>
119. Soret, L., Gérard, J.C., Libert, L., Shematovich, V.I., Bisikalo, D.V., Stiepen, A., Bertaux, J.L.: SPICAM observations and modeling of Mars aurorae. *Icarus* **264**, 398–406 (2016). DOI 10.1016/j.icarus.2015.09.023
120. Spiga, A., Faure, J., Madeleine, J.B., Määttänen, A., Forget, F.: Rocket dust storms and detached dust layers in the Martian atmosphere. *Journal of Geophysical Research (Planets)* **118**, 746–767 (2013). DOI 10.1002/jgre.20046
121. Spiga, A., González-Galindo, F., López-Valverde, M.Á., Forget, F.: Gravity waves, cold pockets and CO<sub>2</sub> clouds in the Martian mesosphere. *Geophys. Res. Lett.* **39**, L02201 (2012). DOI 10.1029/2011GL050343
122. Stevens, M.H., Evans, J.S., Schneider, N.M., Stewart, A.I.F., Deighan, J., Jain, S.K., Crismani, M., Stiepen, A., Chaffin, M.S., McClintock, W.E., Holsclaw, G.M., Lefèvre, F., Lo, D.Y., Clarke, J.T., Montmessin, F., Bougher, S.W., Jakosky, B.M.: New observations of molecular nitrogen in the Martian upper atmosphere by IUVS on MAVEN. *Geophys. Res. Lett.* **42**, 9050–9056 (2015). DOI 10.1002/2015GL065319
123. Stevens, M.H., Siskind, D.E., Evans, J.S., Jain, S.K., Schneider, N.M., Deighan, J., Stewart, A.I.F., Crismani, M., Stiepen, A., Chaffin, M.S., McClintock, W.E., Holsclaw, G.M., Lefvre, F., Lo, D.Y., Clarke, J.T., Montmessin, F., Jakosky, B.M.: Martian mesospheric cloud observations by iuvs on maven: Thermal tides coupled to the upper atmosphere. *Geophysical Research Letters* (2017). DOI 10.1002/2017GL072717. URL <http://dx.doi.org/10.1002/2017GL072717>. 2017GL072717
124. Stewart, A.I.F., Alexander, M.J., Meier, R.R., Paxton, L.J., Bougher, S.W., Fesen, C.G.: Atomic oxygen in the martian thermosphere. *J. Geophys. Res.* **97**, 91–102 (1992). DOI 10.1029/91JA02489
125. Stiepen, A., Gérard, J.C., Gagné, M.É., Montmessin, F., Bertaux, J.L.: Ten years of Martian nitric oxide nightglow observations. *Geophys. Res. Lett.* **42**, 720–725 (2015). DOI 10.1002/2014GL062300

126. Stiepen, A., Jain, S.K., Schneider, N.M., Deighan, J.I., Gonzalez-Galindo, F., Grard, J.C., Milby, Z., Stevens, M.H., Bougher, S., Evans, J.S., Stewart, A.I.F., Chaffin, M.S., Crismani, M., McClintock, W.E., Clarke, J.T., Holsclaw, G.M., Montmessin, F., Lefvre, F., Forget, F., Lo, D.Y., Hubert, B., Jakosky, B.M.: Nitric oxide nightglow and martian mesospheric circulation from maven/iuvs observations and lmd-mgcm predictions. *Journal of Geophysical Research: Space Physics* **122**(5), 5782–5797 (2017). DOI 10.1002/2016JA023523. URL <http://dx.doi.org/10.1002/2016JA023523>.
127. Strobel, D.F.: Aeronomic Systems on Planets, Moons, and Comets. In: Mendillo, M., Nagy, A., & Waite, J. H. (ed.) *Atmospheres in the Solar System: Comparative Aeronomy*, pp. 7–+ (2002)
128. Terada, N., Leblanc, F., Nakagawa, H., Medvedev, A.S., Yi?it, E., Kuroda, T., Hara, T., England, S.L., Fujiwara, H., Terada, K., Seki, K., Mahaffy, P.R., Elrod, M., Benna, M., Grebowsky, J., Jakosky, B.M.: Global distribution and parameter dependences of gravity wave activity in the martian upper thermosphere derived from maven/ngims observations. *Journal of Geophysical Research: Space Physics* **122**(2), 2374–2397 (2017). DOI 10.1002/2016JA023476. URL <http://dx.doi.org/10.1002/2016JA023476>.
129. Thomas, I.R., Vandaele, A.C., Robert, S., Neefs, E., Drummond, R., Daerden, F., Delanoye, S., Ristic, B., Berkenbosch, S., Clairquin, R., Maes, J., Bonnewijn, S., Depiesse, C., Mahieux, A., Trompet, L., Neary, L., Willame, Y., Wilquet, V., Nevejans, D., Aballea, L., Moelans, W., De Vos, L., Lesschaeve, S., Van Vooren, N., Lopez-Moreno, J.J., Patel, M.R., Bellucci, G., Vandaele, A.C., Moreno, L., Juan, J., Bellucci, G., Patel, M., Allen, M., Altieri, F., Aoki, S., Bolsee, D., Clancy, T., Cloutis, E., Daerden, F., Depiesse, C., Fedorova, A., Formisano, V., Funke, B., Fussen, D., Garcia-Comas, M., Geminale, A., Gerard, J.C., Gillotay, D., Giuranna, M., Gonzalez-Galindo, F., Ignatiev, N., Kaminski, J., Karatekin, O., Kasaba, Y., Lefevre, F., Lewis, S., Lopez-Puertas, M., Lopez-Valverde, M.A., Mahieux, A., Mason, J., McConnell, J., Mumma, M., Neary, L., Neefs, E., Novak, R., Renotte, E., Robert, S., Sindoni, G., Smith, M., Thomas, I.R., Trokhimovsky, S., Vander Auwera, J., Villanueva, G., Whiteway, J., Willame, Y., Wilquet, V., Wolff, M., Alonso-Rodrigo, G., Aparicio, d.M.B., Barzin, P., BenMoussa, A., Berkenbosch, S., Biondi, D., Bonnewijn, S., Candini, G.P., Clairquin, R., Cubas, J., Delanoye, S., Giordanengo, B., Gissot, S., Gomez, A., Zafra, J.J., Leese, M., Maes, J., Mazy, E., Mazzoli, A., Meseguer, J., Morales, R., Orban, A., Pastor-Morales, M.d.C., Perez-Grande, I., Ristic, B., Rodriguez-Gomez, J., Saggin, B., Samain, V., Sanz Andres, A., Sanz, R., Simar, J.F., Thibert, T., Team, N.: Optical and radiometric models of the NOMAD instrument part II: the infrared channels - SO and LNO. *OPTICS EXPRESS* **24**(4), 3790–3805 (2016). DOI 10.1364/OE.24.003790. URL <http://www.opticsexpress.org/abstract.cfm?URI=oe-24-4-3790>
130. Titov, D., Bibring, J.P., Cardesin, A., Duxbury, T., Forget, F., Giuranna, M., González-Galindo, F., Holmström, M., Jaumann, R., Määttänen, A., Martin, P., Montmessin, F., Orosei, R., Pätzold, M., Plaut, J., MEx SGS Team: Mars Express recent findings and future plans. In: EGU General Assembly Conference Abstracts, *EGU General Assembly Conference Abstracts*, vol. 19,

- p. 15392 (2017)
131. Vandaele, A., and the NOMAD Team: Nomad, an integrated suite of three spectrometers for the exomars trace gas mission: technical description, science objectives and expected performances. *Space Sci. Rev* **9999**(submitted) (2017)
  132. Vandaele, A., Neefs, E., Drummond, R., Thomas, I., Daerden, F., Lopez-Moreno, J.J., Rodriguez, J., Patel, M., Bellucci, G., Allen, M., Altieri, F., Bolse, D., Clancy, T., Delanoye, S., Depiesse, C., Cloutis, E., Fedorova, A., Formisano, V., Funke, B., Fussen, D., Geminale, A., Grard, J.C., Giuranna, M., Ignatiev, N., Kaminski, J., Karatekin, O., Lefvre, F., Lopez-Puertas, M., Lopez-Valverde, M., Mahieux, A., McConnell, J., Mumma, M., Neary, L., Renotte, E., Ristic, B., Robert, S., Smith, M., Trokhimovsky, S., Auwera, J.V., Villanueva, G., Whiteway, J., Wilquet, V., Wolff, M.: Science objectives and performances of nomad, a spectrometer suite for the exomars {TGO} mission. *Planet. Space Sci.* **119**, 233 – 249 (2015). DOI 10.1016/j.pss.2015.10.003. URL <http://www.sciencedirect.com/science/article/pii/S0032063315003025>
  133. Vandaele, A.C., Willame, Y., Depiesse, C., Thomas, I.R., Robert, S., Bolsée, D., Patel, M.R., Mason, J.P., Leese, M., Lesschaeve, S., Antoine, P., Daerden, F., Delanoye, S., Drummond, R., Neefs, E., Ristic, B., Lopez-Moreno, J.J., Bellucci, G., Team, N.: Optical and radiometric models of the nomad instrument part i: the uvis channel. *Opt. Express* **23**(23), 30,028–30,042 (2015). DOI 10.1364/OE.23.030028. URL <http://www.opticsexpress.org/abstract.cfm?URI=oe-23-23-30028>
  134. Villanueva, G.L., Altieri, F., Clancy, R.T., Encrenaz, T., Fouchet, T., Harogh, P., Lellouch, E., Lopez-Valverde, M.A., Mumma, M.J., Novak, R.E., Smith, M.D., Vandaele, A.C., Wolff, M.J., Ferruit, P., Milam, S.N.: Unique spectroscopy and imaging of mars with the james webb space telescope. *Publications of the Astronomical Society of the Pacific* **128**(959), 018,004 (2016). DOI 10.1088/1538-3873/128/959/018004. URL <http://stacks.iop.org/1538-3873/128/i=959/a=018004>
  135. Wang, L., Fritts, D.C., Tolson, R.H.: Nonmigrating tides inferred from the mars odyssey and mars global surveyor aerobraking data. *Geophysical Research Letters* **33**(23) (2006). DOI 10.1029/2006GL027753. URL <http://dx.doi.org/10.1029/2006GL027753>. L23201
  136. Wilquet, V., Fedorova, A., Montmessin, F., Drummond, R., Mahieux, A., Vandaele, A.C., Villard, E., Korablev, O., Bertaux, J.L.: Preliminary characterization of the upper haze by SPICAV/SOIR solar occultation in UV to mid-IR onboard Venus Express. *Journal of Geophysical Research (Planets)* **114**, E00B42 (2009). DOI 10.1029/2008JE003186
  137. Wilson, R.J., Guzewich, S.D.: Influence of water ice clouds on nighttime tropical temperature structure as seen by the mars climate sounder. *Geophysical Research Letters* **41**(10), 3375–3381 (2014). DOI 10.1002/2014GL060086. URL <http://dx.doi.org/10.1002/2014GL060086>. 2014GL060086
  138. Wilson, R.J., Neumann, G.A., Smith, M.D.: Diurnal variation and radiative influence of martian water ice clouds. *Geophysical Research Letters* **34**(2) (2007). DOI 10.1029/2006GL027976. URL <http://dx.doi.org/10.1029/2006GL027976>. L02710

139. Withers, P.: Mars global surveyor and mars odyssey accelerometer observations of the martian upper atmosphere during aerobraking. *Geophysical Research Letters* **33**(2) (2006). DOI 10.1029/2005GL024447. URL <http://dx.doi.org/10.1029/2005GL024447>. L02201
140. Withers, P., Bougher, S.W., Keating, G.M.: The effects of topographically-controlled thermal tides in the martian upper atmosphere as seen by the mgs accelerometer. *Icarus* **164**, 14–32 (2003). DOI 10.1016/S0019-1035(03)00135-0
141. Wolff, M., López-Valverde, M.A., Madeleine, J.B., J., W.R., M., S., Foucher, F., Delory, G.: Chapter 6 - radiative processes: Techniques and applications. In: B. Haberle, M. Smith, T. Clancy, F. Forget., R. Zurek (eds.) *The Atmosphere and Climate of Mars*, pp. 106–171. Cambridge University Press (2017). DOI 10.1017/9781139060172. URL [www.cambridge.org/9781107016187](http://www.cambridge.org/9781107016187)
142. Wolff, M.J., Clancy, R.T., Cantor, B.A.: Four Mars Years of Mapping Water Ice Clouds with MRO/MARCI. *AGU Fall Meeting Abstracts* (2013)
143. Wolff, M.J., Clancy, R.T., Goguen, J.D., Malin, M.C., Cantor, B.A.: Ultraviolet dust aerosol properties as observed by {MARCI}. *Icarus* **208**(1), 143 – 155 (2010). DOI <https://doi.org/10.1016/j.icarus.2010.01.010>. URL <http://www.sciencedirect.com/science/article/pii/S0019103510000205>
144. Wolff, M.J., Smith, M.D., Clancy, R.T., Arvidson, R., Kahre, M., Seelos, F., Murchie, S., Savijrvi, H.: Wavelength dependence of dust aerosol single scattering albedo as observed by the compact reconnaissance imaging spectrometer. *Journal of Geophysical Research: Planets* **114**(E2) (2009). DOI 10.1029/2009JE003350. URL <http://dx.doi.org/10.1029/2009JE003350>. E00D04
145. Yigit, E., England, S.L., Liu, G., Medvedev, A.S., Mahaffy, P.R., Kuroda, T., Jakosky, B.M.: High-altitude gravity waves in the Martian thermosphere observed by MAVEN/NGIMS and modeled by a gravity wave scheme. *Geophys. Res. Lett.* **42**, 8993–9000 (2015). DOI 10.1002/2015GL065307
146. Zurek, R.W., Tolson, R.A., Bougher, S.W., Lugo, R.A., Baird, D.T., Bell, J.M., Jakosky, B.M.: Mars thermosphere as seen in maven accelerometer data. *Journal of Geophysical Research: Space Physics* **122**(3), 3798–3814 (2017). DOI 10.1002/2016JA023641. URL <http://dx.doi.org/10.1002/2016JA023641>. 2016JA023641
147. Zurek, R.W., Tolson, R.H., Baird, D., Johnson, M.Z., Bougher, S.W.: Application of maven accelerometer and attitude control data to mars atmospheric characterization. *Space Science Reviews* **195**(1), 303–317 (2015). DOI 10.1007/s11214-014-0095-x. URL <http://dx.doi.org/10.1007/s11214-014-0095-x>